 doi.org/10.52568/002046/JCSP/48.03.2026

Computational Insights of Completely Non-Fused Ring Acceptor through Synergetic Engineering of Terminal Acceptors for Stable and Effective Organic Solar Cells

[1]Tahira Faiz, [1]Haq Nawaz Bhatti, [1,2]Javed Iqbal** and [3]Muhammad Yaseen
[1]*Department of Chemistry, University of Agriculture, Faisalabad.*
[2]*Department of Chemistry, College of Science, University of Bahrain, Sakhir, Kingdom of Bahrain.*
[2]*Department of Physics, University of Agriculture, Faisalabad.*
haq_nawaz@uaf.edu.pk*, Javedkhattak79@gmail.com**

(Received on 12th March 2025, accepted in revised form 22nd August 2025)

Summary: The development of stable and efficient solar cells with high power conversion efficiency is a subtle challenge. To compete by attaining a decreased band gap and uplifted power conversion efficiency, five new molecules (PM1-PM5) are formulated through the synergetic engineering of the terminal acceptor. The bond angle of the molecules PM1-PM5 ranges from (0.09 – 1.78 θ°) and the bond length (1.41 – 1.43 Å). The computed molecules highlighted promising outcomes with a lowered band gap, bathochromic shift in absorption spectra, excellent excitation phenomenon, lower exciton binding energy, prominent LHE, and sufficient open circuit voltage required for commercialization. The MPW1PW91 functional with 6-31 G (d, p) methodology is selected for computational analysis. Among all customized chromophores, PM4 and PM5 manifested the lowest band gap (2.09 eV), absorption at 773 and 776 nm, and decreased excitation energy (1.60 eV). PM1 and PM4 demonstrated the highest dipole moment (13.22 D and 12.80 D in chloroform solvent). Furthermore, PM1 and PM2 outperformed in light-harvesting potential and manifested better charge transfer owing to their reduced reorganization energy of electrons and holes. Of all the designed molecules PM2, PM3, and PM4 (96.33, 96.43, 97.99) have the high NTOs percentage, showing their highest excitation of the electrons. The oscillatory strength of the molecules has values from 1.8043 to 2.8974. The comparable V_{OC} (1.34-1.56 eV) was obtained by blending investigated chromophores with a PCBM acceptor. The percentage contribution of the donor, spacer, and acceptor shows that the highest donor contribution is given by the PM2 (HOMO 60.2% and LUMO 47.3%), while the spacer contribution is given by the PM5 (21.7% and 80.3%) and the acceptor contribution is highest by the PM2 (HOMO22.8% and 17.1%). To describe this in words, all individual molecules are well made with measured electron and photoelectric parameters and are provided as stable and sufficient materials to transport holes developed for the marketing of solar devices.

Graphical Abstract

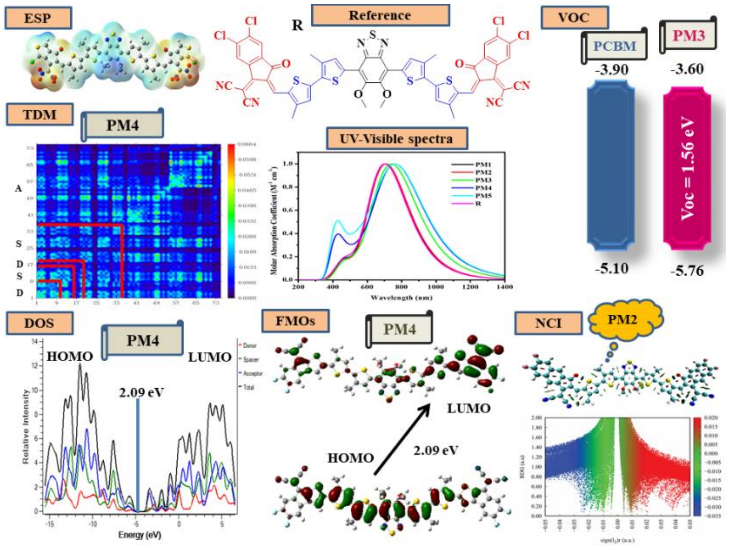

Keywords: Frontier molecular orbitals, Synergetic engineering of terminal acceptors, Non-covalent interaction, Transition density matrix

***To whom all correspondence should be addressed.**

Introduction

Organic solar cells (OSCs) have attained prominent attraction as emerging technology, specifically credited to consequential stability under incessant thermal exposure and generation of electrical energy at extremely low cost[1]. Among the various available inexhaustible energy resources, solar energy is considered as eco-friendly, reliable and carbon neutral one[2]. For decades, silicon based solar cells potentially converted solar energy into valuable electrical ones with elevated photo-to-electric conversion capability[3]. The large scaled applications of silicon based solar devices seeming to be limited owing to their shortcomings like inflexible morphology, heavy, highly expensive, producers of carbon emissions as pollution[4]. Subsequently, revolution and leapfrog development in the photovoltaic technology has been observed in their organic counterparts. Henceforth, various potential implementations in materials science, materials manufacturing and mechanics have elevated of prominence of OSCs in solar forthcoming technologies[5].

The device workability of bulk-heterojunction solar cells is linked with nature of electrodes, hole and electron transporting layer and incident photon absorbing active layer of organic materials[6]. The potential and effective active layer of bulk-heterojunction solar cells is generated by intermingling of acceptor materials having high electron affinity with typical robust donor materials exhibiting low ionizing potential[7]. It is imperative to afford proper morphological arrangement to attain better donor/acceptor interfacial area and smaller exciton diffusion range for captivating light response for development of sufficient opto-electric current resulted in significant breakthroughs in PCEs[8].

The constrained functionality of fullerene acceptors (FAs) resulted by various challenges, concerning unstable chemical morphology, chemical changes, restricted upgradeable energy levels, and weak absorption spectra in UV-visible region and near infrared region[9]. For the sake of complications and attainment of widespread spectrum for exploring crucial optoelectronic properties and charge carrier mobilities, non-fullerene acceptors (NFAs) are significantly preferred[10]. The unending and outshined growth of fullerene free acceptors revolutionized in photovoltaic performance credited to broad light absorption, full spectral coverage, inadequate occupancy of electrons, enhanced thermal stability, variable energy levels and improved light harvesting efficiency that empowered them to attain PCE over 17 %[11].

Fused ring electron acceptors have high power conversion efficiency unlike the acceptor-donor-acceptor traditional structures gives good planarity and guarantee of rigidity to solar devices[12]. Fused ring acceptors have efficiency but they are complicated in synthesis and take much time for formation due to multiple synthesis processes and also have low product yield[13]. In contrast to the fused ring acceptors, the non-fused ring electrons acceptors (NFREAs) are linked by the single bond to the adjacent units in the molecules having high reaction yield with a simple synthesis procedure[14]. To maintain the NFREAs, major strategies are the introduction of heteroatoms in the fused rings to prevent the twisting of the single bond by creating the hindrance in side chains, conformational stability, and chemical structures[15]. Both these features can be controlled by the higher possibility of rotation of NFREAs[16]. The NFREAs can reduce the OSCs' cost by simplifying the complicated synthesis method and increasing the product yield[17]. Due to the low-cost yield in the solar cells, NFREAs become promising in manufacturing high-performance OSCs[18].

Various molecular strategies are developed to fine tune energy levels for convenient charge transfer essential for forthcoming commercialization[19]. Proper molecular designing of molecular structure is considered as effective way to modify organic photovoltaic materials to enhance intramolecular interaction[20]. In various scientific literatures, careful adjustment in the molecular size, functionalization, planarity and structural geometry containing conjugated fused rings substantially influenced the competencies of optoelectronic properties[21]. The introduction of proficient electron withdrawing acceptors is considered as molecular motif for engineering techniques for efficient planning of non-fullerene acceptors that captivate the photovoltaic performance of molecular frameworks[22]. Furthermore, end-group amelioration tune the intermolecular attractions of chromophores, effectively lowers energy loss by facilitating ordered packing of the molecules[23].

Chenyang Hen and co-workers had synthesized the BTZT-4ClR (named as R reference molecule) completely non-fused ring acceptors (Y-series) by inspiring the A-D-A-D-A which contained the non-fused thiophene and alkoxy substitution[24].

BTZT-4ClR exhibits an outstanding efficiency of 15.41 %, a remarkable $V_{OC\ of}$ 0.964 V, a high value of the FF 0.731, and with significantly improved J_{SC} of 20.12 mA cm^{-2} [25]. By using R as reference molecule, five different compounds are designed designated as PM1-PM5. In this modification, end-capped acceptors are removed and replaced with five different new acceptors to check and enhance the efficacy, stability, and PCE. Through computational approach, various parameters like band gap, absorption maxima, excitation energy, dipole moment, reorganization energy, fill factor and open circuit voltage are determined[26].

Computational Methodology

We have drawn a total of six structures one is reference molecule R and five other derivatives named as PM1-PM5 which are derived from reference. The structural manifestation was performed by implementing ChemDraw software[27]. GaussView 6.0 software is employed to design 3D structural geometries of all chromophores[28], and Gaussian 09 software is applied to investigate mathematical and statistical calculations of the reference and designed molecules[29]. To calculate electronic, thermodynamic, and spectroscopic properties, density functional theory (DFT) and time-dependent density functional theory (TD-DFT) are utilized[30]. To obtain UV-visible maxima we used different functionals that authenticate wellness of DFT level of theory for newly designed molecules and its graphical visualization is examined in Fig 1 while summarized values are tabulated in Table 1.

By applying four different functionals "B3LYP", "CAM-B3LYP", "MPW1PW91" and "ωB97XD" of DFT with 6-31G (d,p) basis set, for the energy calculations followed by the TD-DFT on the reference molecule, we selected the MPW1PW91functional because it gives the lowermost wavelength at ground state[31]. All further analysis was done by using MPW1PW91 method as a base. The model I have used for solvent phase calculations is IEFPCM (Integral Equation Formalism Polarizable Continuum Model). The Polarizable Continuum Model (PCM) using the integral equation formalism variant (IEFPCM) is the default SCRF method. This method creates the solute cavity via a set of overlapping spheres. The calculated values of the HOMO and LUMO of the four different functionals are applied given in the Table 2.

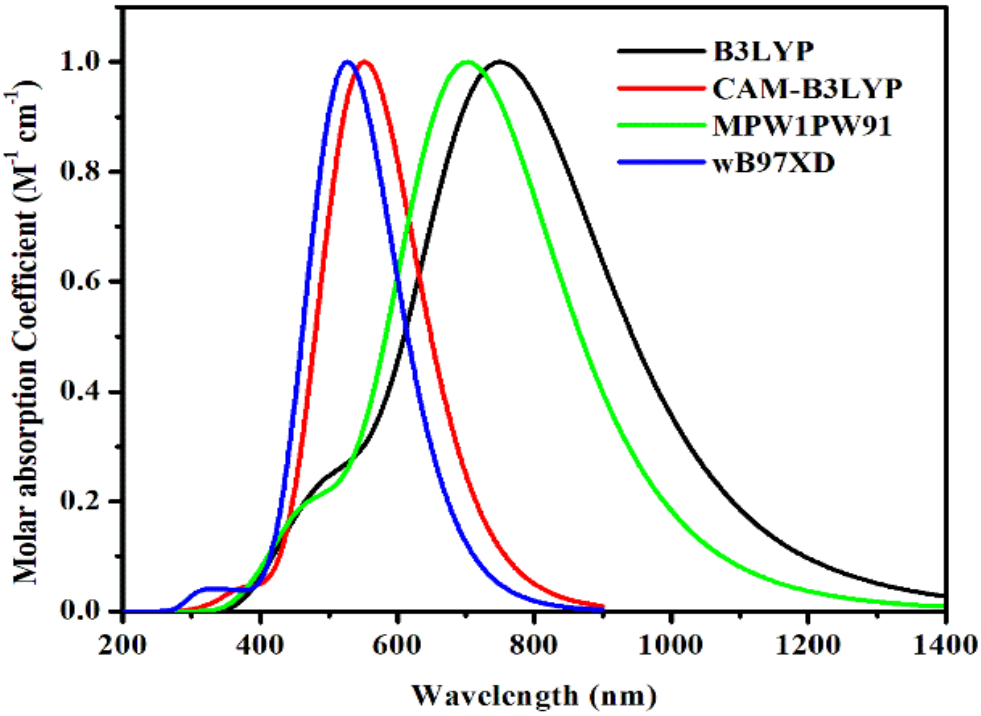

Fig 1: Visualization of absorption spectra of reference (R) molecule for different functional plotted by aiding Origin 6.0 software.

Table-1: Concise values of λ_{max} utilizing four functional for selection and implementation of most appropriate functional.

Functionals	Experimental λ_{max} (nm)	Calculated λ_{max} (nm)
B3LYP	**667**	**755**
CAM-B3LYP	**-**	**532**
MPW1PW91	**-**	**705**
wB97XD	**-**	**529**

Table-2: The HOMO and LUMO values of the four different functionals.

Functionals	HOMO	LUMO
B3LYP	**0.2092**	**0.1314**
CAM-B3LYP	**0.2445**	**0.09223**
MPW1PW91	**0.2131**	**0.1303**
wB97XD	**0.2663**	**0.0737**

All other calculations FMOs, DOS, TDM, and charge transport analysis were performed at the DFT level by implementing the MPW1PW91/6-31G(d,p) level of theory. By employing equation 1, inter and internal charge transmission can be calculated[32].

$$\lambda_{total} = \lambda_h + \lambda_0 \quad (1)$$

The reorganization energy (RE) represents both internal reorganization energy (IR) as well as external reorganization energy (ER) integral spheres[33]. IR explains and deals with all the geometric changes that occur in the molecule inside during the charge transformation[34], they deal with the change in bond lengths and bond angles while ER explains solvation changes that occurred during the charge transformations. In our recent investigation, external reorganization energy is excluded due to negligible impact and main concern is on internal reorganization energy[35]. To demonstrate the transfer rates of the electrons and holes during charge transfer, equations 2 and 3 are predominantly used[36].

$$\lambda_e = [E_0^- - E_-] + [E^0_- - E_0] \quad (2)$$

$$\lambda_h = [E^+_0 - E_+] + [E^0_+ - E_0] \quad (3)$$

In the above-mentioned equations, E_0, E_0^- and E_0^+ represents ground state energies at 0, -1 and +1 charges respectively determined through optimized neutral geometry. E_+ and E_- are determined by optimized structures of cation and anion correspondingly. While E^0_+ and E^0_- are the neutral molecular energies of cation and anion calculated by optimized cationic and anionic optimized molecular configuration.

Results and Discussion

Optimized Molecular Geometry

In order to examine optimized geometric consideration, reference and customized chromophores are partitioned into three segments; central donor core (black), alkyl substituted di-thiophene as linking groups (blue) while substituted acceptors (red) at terminal vicinity. The 2D geometric configuration is visualized in Fig 2 which is drawn from ChemDraw 8.0 software[37] . The optimized molecular configuration of all the chromophores is eventually performed under MPW1PW91 basis functional and evaluation of bond length and dihedral angle is considered to validate their prominent behavior. The analysis of dihedral angle and bond length is critical in order to analyze the planarity elucidation and extended conjugation in the molecules which is vital for better charge transference and elevated absorption of solar radiations. It is further examined how molecules are oriented in the plane after its optimization and its impact on geometry which is essential to develop efficient solar cells[38] .

The bond length at the site of attachment signifies conjugation within the chromophores and is analyzed to understand this phenomenon. From careful investigation, bond length of all chromophores is ranging from 1.41-1.43 Å which lies between singly bonded (C−C) and doubly bonded (C=C) atoms which demonstrates that prominent conjugation is present in the customized

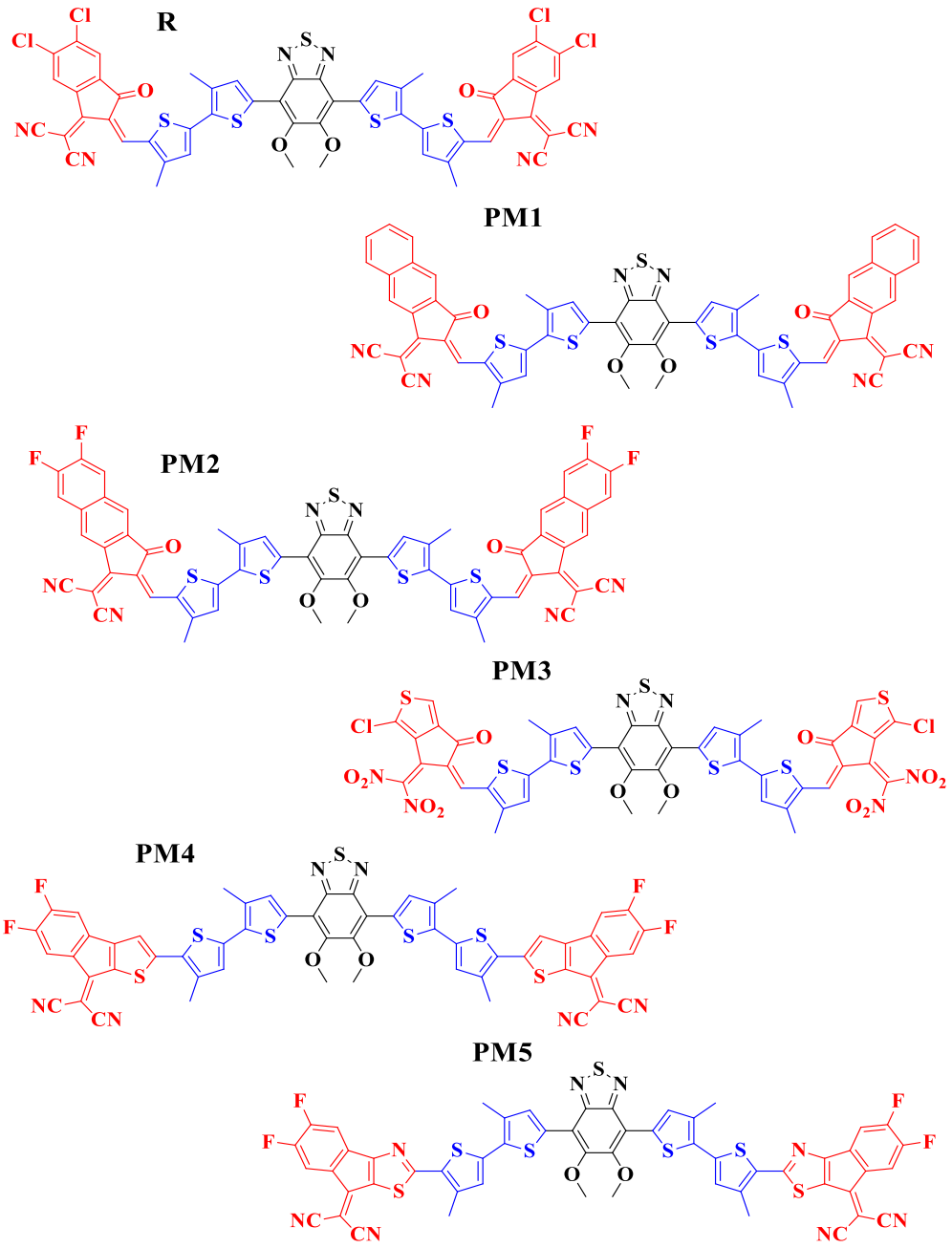

Fig 2: 2D molecular geometric configurations of R and PM1-PM5 molecules drawn by utilizing ChemDraw 7.0 software. molecules. Another plausible parameter that must be evaluated is dihedral angle which transcribes planar character and transmission nature of electrical charges[39] . It is directly concerned with planar configuration, highlighting that reduced dihedral angle at the attachment site enhances planarity and charge transmission. The dihedral angle of the chromophore ranges from 0.03° - 1.78°. The declining order of dihedral angle of reference (R) and planned molecules (PM1-PM5) is given as; PM4 > PM3 > PM2 > R > PM1 > PM5. To sum up, it is clearly demonstrated in Table 3 and Fig 3, all planned chromophores have negligible dihedral angle after optimization predicting their almost planar configuration which is aided in charge dispersal and their potential to reach at respective electrodes vital of commercialization[40] .

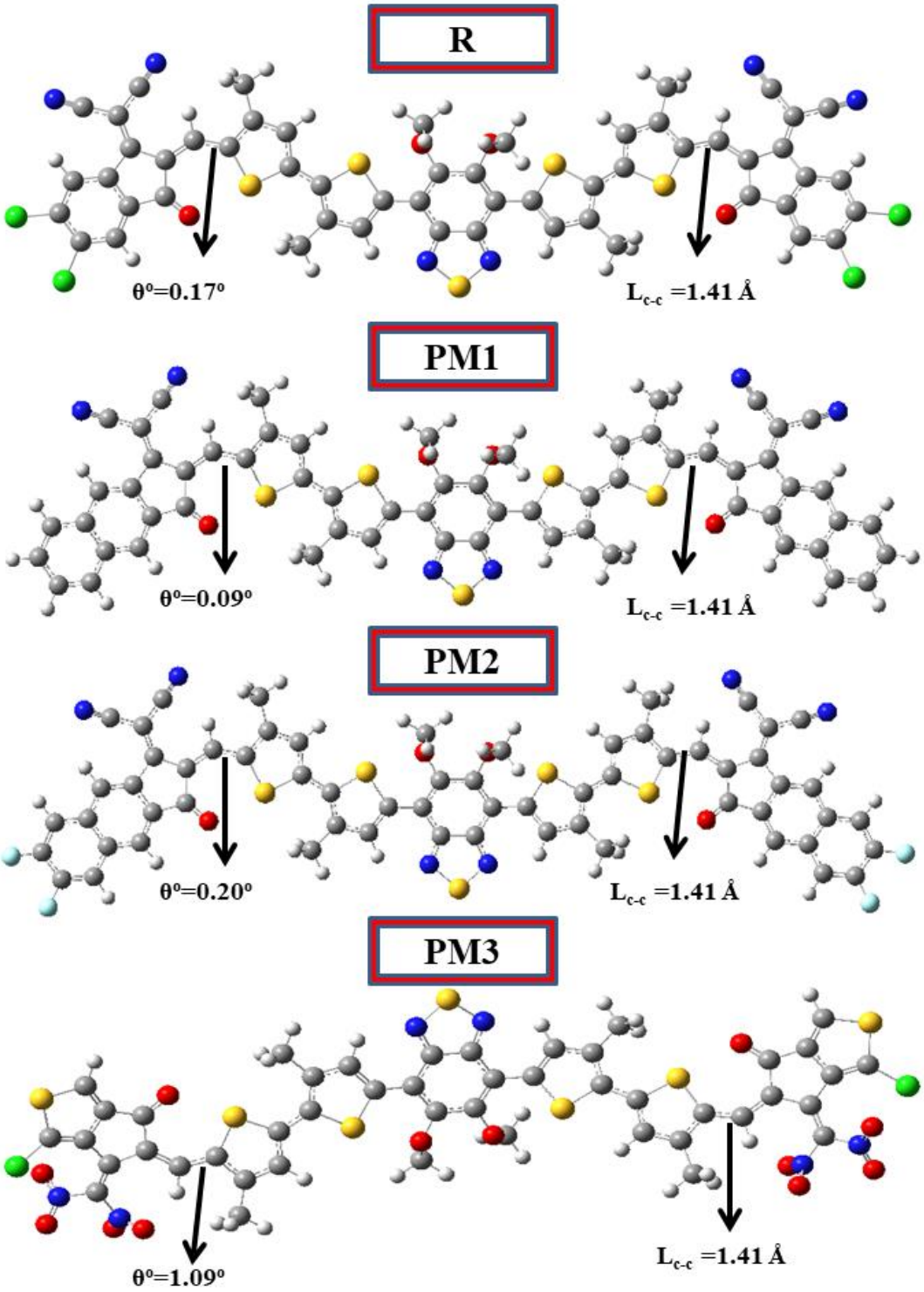
R
θ°=0.17°
L_{c-c} =1.41 Å
PM1
θ°=0.09°
L_{c-c} =1.41 Å
PM2
θ°=0.20°
L_{c-c} =1.41 Å
PM3
θ°=1.09°
L_{c-c} =1.41 Å

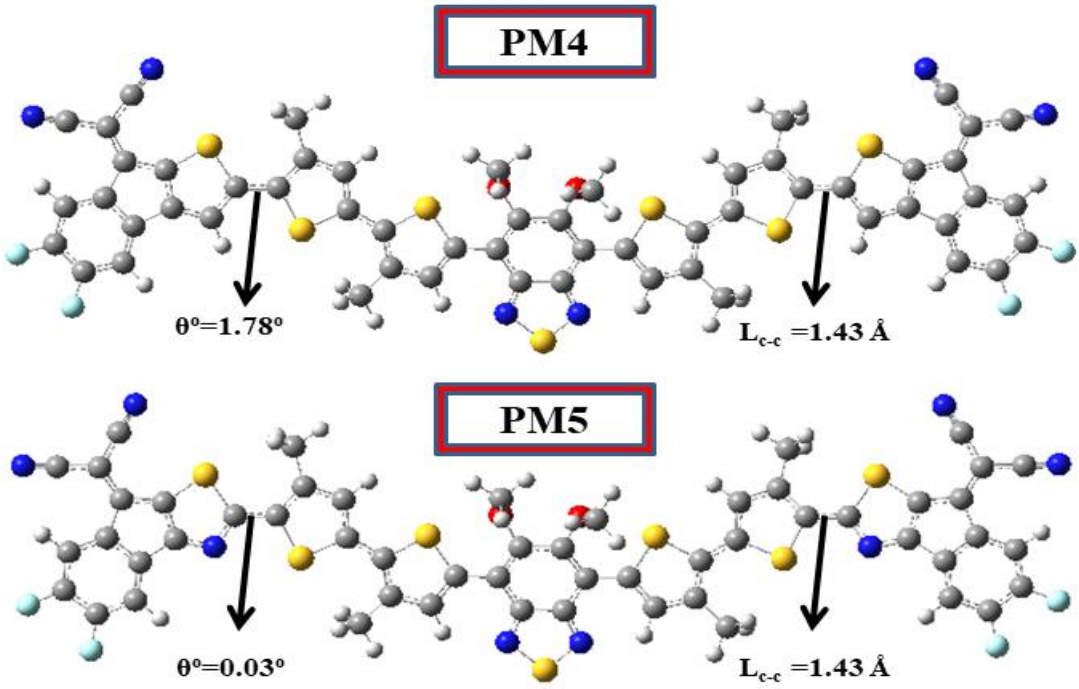

Fig 3: Visual portray of optimized molecular configurations along with computed bond length and dihedral angle of R and PM1-PM5 chromophores

Table 3: Summarized values of bond length and dihedral angle of R and PM1-PM5 predicting conjugation and planar configuration

Molecules	Bond length (Å)	Bond angle (θ°)
R	**1.41**	**0.17**
PM1	**1.41**	**0.09**
PM2	**1.41**	**0.20**
PM3	**1.41**	**1.09**
PM4	**1.43**	**1.78**
PM5	**1.43**	**0.03**

Frontier Molecular Orbital (FMOs) Consideration

Analysis of FMOs is a pivotal parameter which is eminent theoretical approach to calculate the electronic density distribution, charge transmission, and electronic properties estimation, which are calculated from ground state geometries of the molecules. To explain the optoelectronic properties and charge transfer of the studied molecules, FMOs analysis at ground state is explored[41] . The charge cloud patterns around the HOMO and LUMO are developed by the intermolecular charge transmission. HOMO is designated as the valence band (VB) while the LUMO is defined as the conduction band (CB). The difference between HOMO and LUMO is known as the band gap or energy gap which is calculated by FMOs analysis provided in equation 4[42] .

$$E_{gap} = E_{LUMO} - E_{HOMO} \quad (4)$$

Here is H_{gap} is the band gap, E_{LUMO} is the energy of the of the electrons at excited state, and E_{HOMO} is the energy of the electrons at ground state. Fig 4 explains the electronic charge density distribution on the surface of the molecules in the form of red and green clouds; red color shows the negative charge while the green color shows the positive charge. HOMO is the donor part of the molecule while LUMO is the acceptor part of the molecule. If the molecules have greater charge concentration, the chances of charge transfer will be increased resulting in captivated efficiency of solar devices[43] .

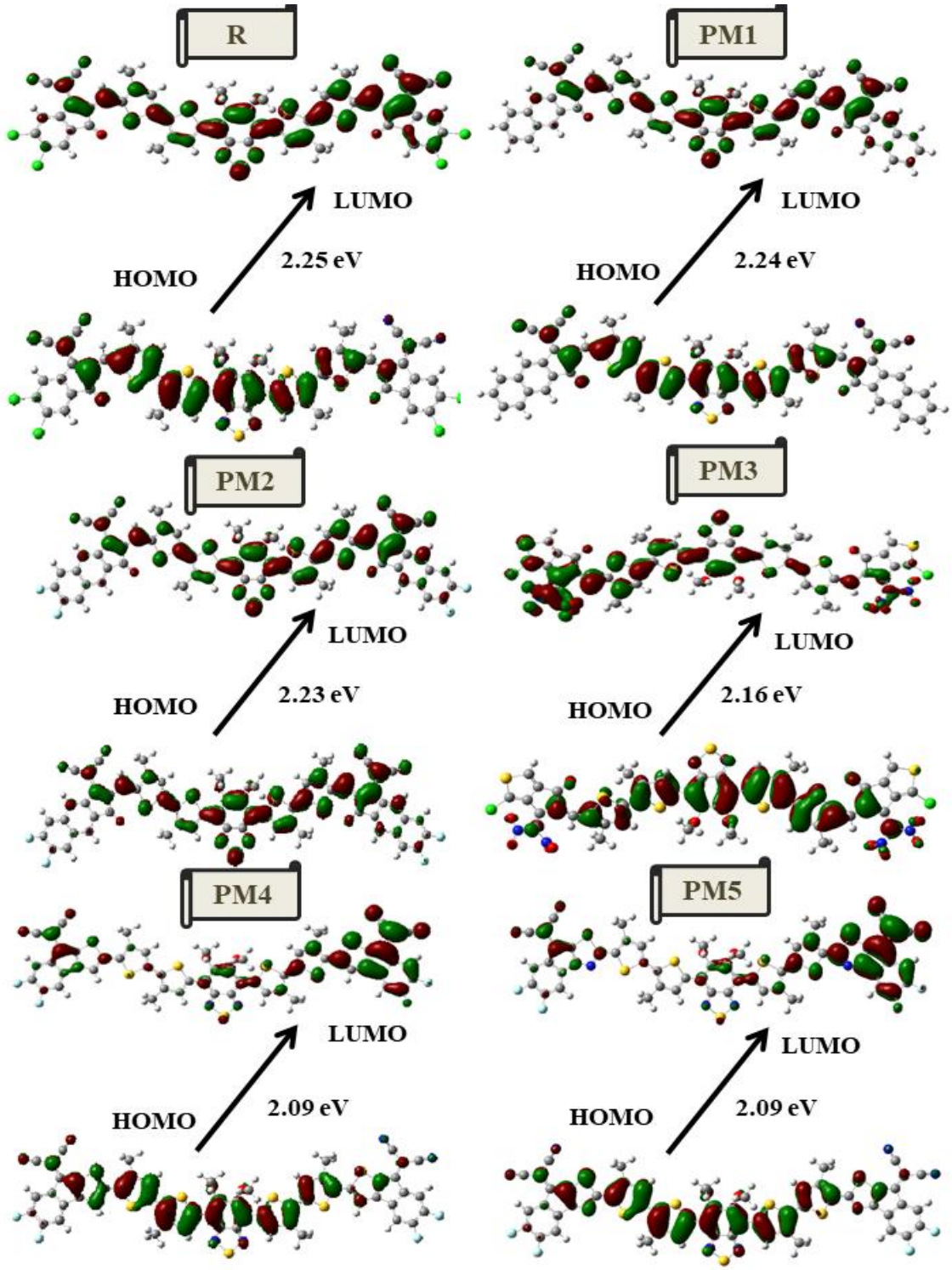

Fig. 4: Illustration of optical band gap along with computed HOMO and LUMO values of all chromophores.

From the recent investigation, reference molecule has HOMO energy level of -5.79 eV while LUMO energy level of -3.54 eV and its photo band gap is 2.25 eV. The scrutinized chromophores (PM1-PM5) have reduced band gap elucidation ranging 2.09-2.24 eV illuminating that substituted acceptors have better potential of withdrawing electrons resulting in facile excitation. The summarized statistical values in Table 4 demonstrate that PM4 and PM5 molecules have better adaptability of excitation phenomenon and photo electronic attributes owing to sufficiently decreased band gap[44] .

Table-4: Computed HOMO and LUMO energy levels along with optical band gap for all scrutinized chromophores

Molecules	HOMO (eV)	LUMO (eV)	E_g (eV)	NTOs%
R	-5.79	-3.54	2.25	95.44
PM1	-5.60	-3.36	2.24	95.55
PM2	-5.70	-3.47	2.23	96.33
PM3	-5.76	-3.60	2.16	96.43
PM4	-5.54	-3.45	2.09	97.99
PM5	-5.64	-3.55	2.09	95.99

Natural transition orbitals (NTOs)

Natural transition orbitals (NTOs) are the best way to explain charge proliferation in the molecules. For this purpose, there should be a great level of excitation between the HOMO and LUMO levels of the chromophores. The main excitation in orbitals of the electron-hole is provided by the NTOs in the molecules which explain that there should be a concise band gap between the HOMO-LUMO energy levels[45] . The molecules with a lot of excitations will work easily with NTOs because they have greater conjugations in the molecules. In charge transference, the electrons move from HOMO to LUMO, HOMO is allocated as a hole because it creates a hole by giving its electrons to the LUMO, while LUMO is designated as a particle because it receives the electrons from HOMO. At the first, excitation energy is very high which is detected by the high oscillator strength. NTO's clearly distinguish the electron density between ground and excited states. In the Fig 5, NTOs structures of the reference and designed molecules explain the electron density distribution over the molecule surface[46].

The highly electronegative groups like cyano, fluoro, carbonyl and methoxy are majorly involved in bathochromic shift of absorption by enhancing the conjugation length within the chromophores. Through various investigations, it is understood that molecule absorbs such type of radiations whose energy level matches with their corresponding band gaps and resulted in excitation of charges[48]. Furthermore, bathochromic absorption predominantly enhances intramolecular charges transfer owing to their better light captivating ability and in turn results in facile excitation phenomenon to proceed[49].

The absorption spectra of all chromophores are plotted at best matched MPW1PW91 functional and its eye-catching view is configured in Figure 6 while summarized results are shown in Table 5 for solvent medium and Table 6 for gaseous phase.

Table 5: Concised values of various optoelectronic parameters (λ_{ma}, E_x, oscillator strength, dipole moment, interaction coefficient) in solvent phase

Molecules	λ_{max} (nm)	E_x (eV)	Oscillator strength	Dipole moment (D)	Interaction Coefficient
R	705	1.76	3.1004	8.55	0.68098
PM1	706	1.76	3.2461	13.22	0.68170
PM2	710	1.75	3.2675	10.34	0.68160
PM3	747	1.66	2.8196	10.56	0.66444
PM4	773	1.60	2.1560	12.80	0.64742
PM5	776	1.60	1.9434	8.47	0.63402

Table 6: Concised values of various optoelectronic parameters (λ_{ma}, E_x, oscillator strength, dipole moment, interaction coefficient) in gaseous phase

Molecules	λ_{max} (nm)	E_x (eV)	Oscillator strength	Dipole moment (D)	Interaction Coefficient
R	671	1.85	2.7664	7.11	0.68509
PM1	676	1.83	2.8612	10.86	0.68473
PM2	679	1.83	2.8974	8.39	0.68436
PM3	695	1.78	2.5615	8.44	0.67580
PM4	719	1.72	1.9737	9.89	0.63108
PM5	721	1.72	1.8043	6.92	0.61578

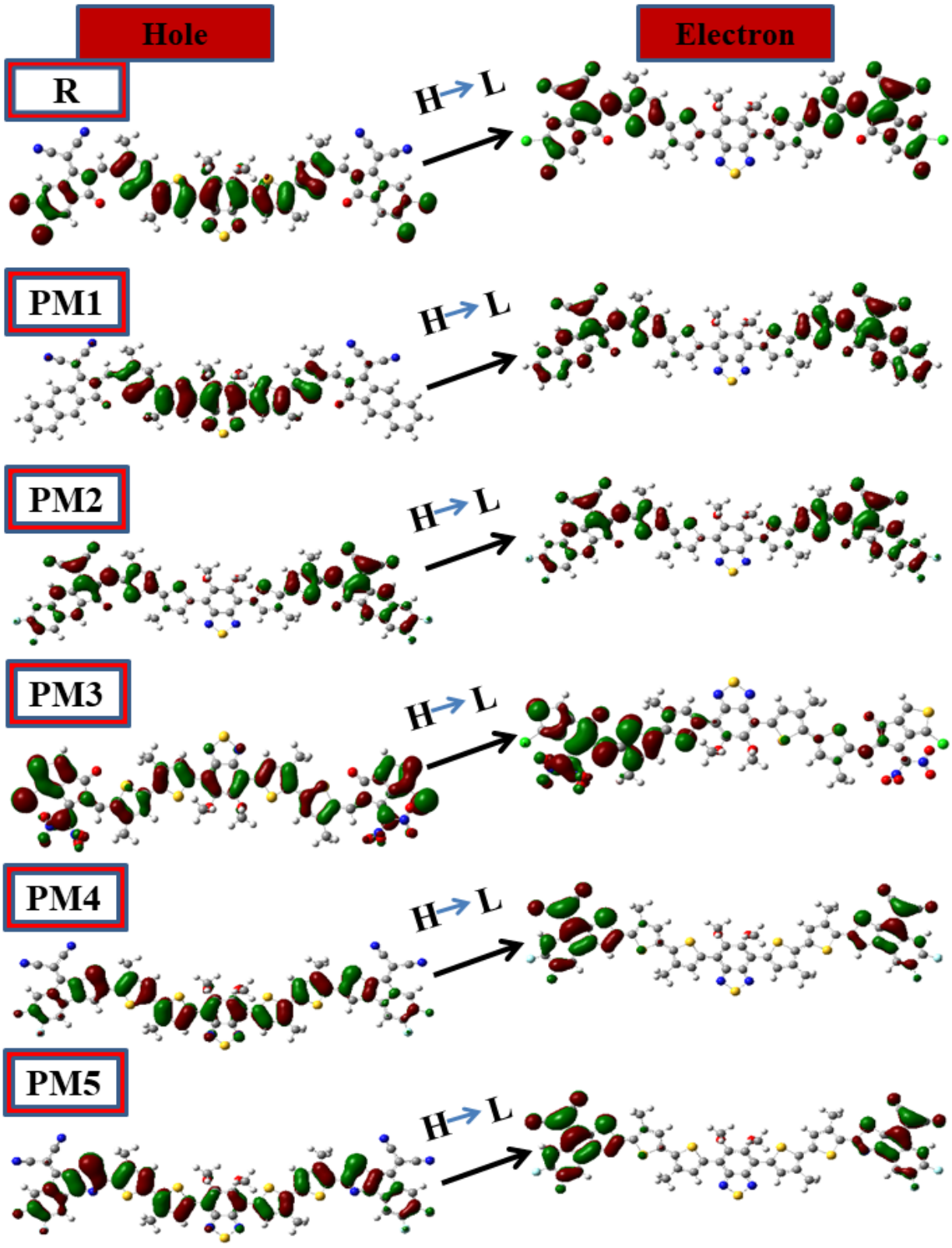

Fig. 5: Picturization of NTO's of reference and investigated molecules (PM1-PM5).

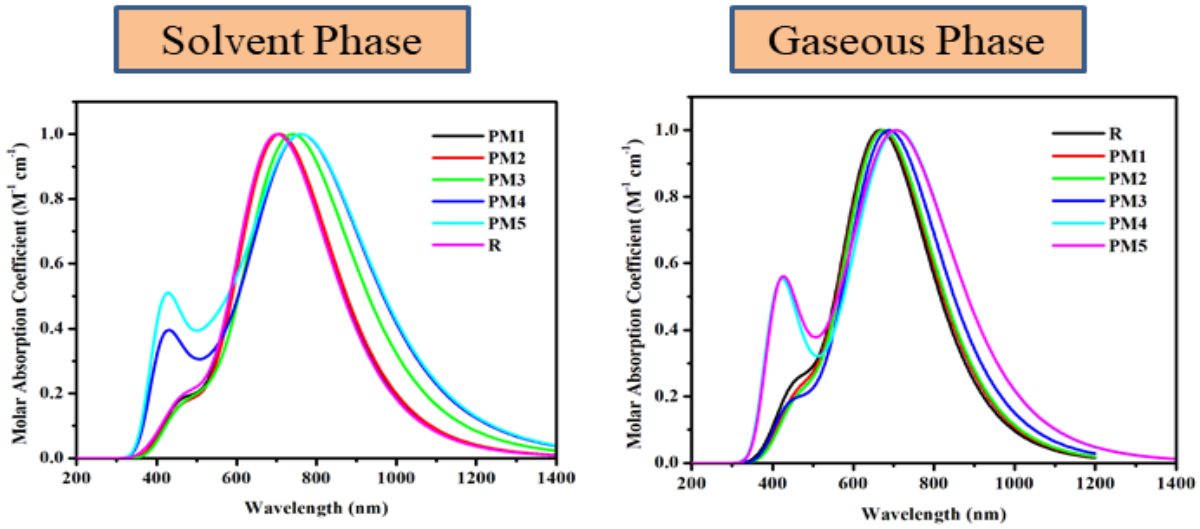

Fig. 6: UV-absorption spectra of R and PM1-PM5 in solvent (left) and gaseous (right) phases.

The highly electronegative groups like cyano, fluoro, carbonyl and methoxy are majorly involved in bathochromic shift of absorption by enhancing the conjugation length within the chromophores. Through various investigations, it is understood that molecule absorbs such type of radiations whose energy level matches with their corresponding band gaps and resulted in excitation of charges[48]. Furthermore, bathochromic absorption predominantly enhances intramolecular charges transfer owing to their better light captivating ability and in turn results in facile excitation phenomenon to proceed[49].

The absorption spectra of all chromophores are plotted at best matched MPW1PW91 functional and its eye-catching view is conFigd in Fig 6 while summarized results are shown in Table 5 for solvent medium and Table 6 for gaseous phase.

The computed wavelength observed by the reference scaffold is 705 nm at solvent phase while 671 nm in gaseous medium[50]. The planned molecules (PM1-PM5) demonstrated maximum absorption ranging from 706-776 nm in chloroform solvent while 676-721 nm in gaseous media. The descending order of absorption in solvent medium is; PM5 > PM4 > PM3 > PM2 > PM1 > R and same trend is illustrated in gaseous medium. To cut in a nutshell, all modified molecules especially PM4 and PM5 have elevated absorption highlighting their effective utilization in prominent solar gadgets[51].

Table-5: Concised values of various optoelectronic parameters (λ_{ma}, E_x, oscillator strength, dipole moment, interaction coefficient) in solvent phase

Molecules	λ_{max} (nm)	E_x (eV)	Oscillator strength	Dipole moment (D)	Interaction Coefficient
R	705	1.76	3.1004	8.55	0.68098
PM1	706	1.76	3.2461	13.22	0.68170
PM2	710	1.75	3.2675	10.34	0.68160
PM3	747	1.66	2.8196	10.56	0.66444
PM4	773	1.60	2.1560	12.80	0.64742
PM5	776	1.60	1.9434	8.47	0.63402

Table-6: Concised values of various optoelectronic parameters (λ_{ma}, E_x, oscillator strength, dipole moment, interaction coefficient) in gaseous phase

Molecules	λ_{max} (nm)	E_x (eV)	Oscillator strength	Dipole moment (D)	Interaction Coefficient
R	671	1.85	2.7664	7.11	0.68509
PM1	676	1.83	2.8612	10.86	0.68473
PM2	679	1.83	2.8974	8.39	0.68436
PM3	695	1.78	2.5615	8.44	0.67580
PM4	719	1.72	1.9737	9.89	0.63108
PM5	721	1.72	1.8043	6.92	0.61578

Another prominent parameter to be evaluated critically is oscillator strength. It correlates directly with band gap considerations. It predominantly transcribes the electronic excitations taking is incredible manner and thus suggests the excellent sites of intramolecular charge transference in the chromophores[52]. Furthermore, it is linked with light harvesting efficiency, increased value of oscillator strength captivated the light harvesting potential and aiding to generate sufficient amount of photo-current. The ascending trend of oscillator strength both chloroform solvent and gaseous media is; PM5 < PM4 < PM3 < R < PM1 < PM2. The statistical considerations summarized in Table 5 and 6 rationally gives a clue that PM1 and PM2 have better light harvesting capability than other chromophores and reference molecules suggesting their better adeptness[53].

Excitation energy and interaction coefficient

The minimum quantity of energy which is essentially required to excite electron from ground (S_0) to first excited state (S_1) is named as first excitation energy. It is concerned with band gap, lower the optical band gap, facile will be excitation phenomenon and vice-versa. It is mandatory; excitation energy must be lowered for the molecules for prominent excitation to take place[54]. The ascending sequence of excitation for all chromophores is; PM5 < PM4 < PM3 < PM2 < PM1 < R. Concised statistical values in Table 5 and 6 prescribes that all investigated chromophores have lower excitation energy and show prominent excitation upon pulling of electronic density and separation of excitons upon absorption of solar radiations, turning their effectiveness in greater extent in solar devices[55].

In order to determine charge transference, interaction coefficient is considered as notable and reliable elucidator. It enables to determine electron-hole coupling. Inverse relation is observed between interaction coefficient and charge transference highlighting that decreased values of interaction coefficient is essential for smooth charge transfer. From Table 5 and 6, all investigated molecules except PM1 and PM2 has lower interaction coefficient which clearly transcribes that charge is effectively shifted within chromophores[55].

Molecular Electrostatic Potential (MEP)

Molecular electrostatic potential separates the charge density within the molecule to identify the electrophilic and nucleophilic regions. It explains the charge transfer from the donating groups to the acceptor groups. Each region on the molecule affects the electronic properties in different ways. The positive potential regions lack electrons while the regions having negative electrostatic potentials have a rich density of electrons, blue and red colors indicate these potions. Based on the electrostatic potential, colored regions are aligned in order from negative to positive electrostatic potentials[56]. The MEP structures of the reference molecule and newly investigated molecules are visualized in Fig 7 which demonstrates that all the molecules show the distribution of the electronic density in the cloud form on the molecules. The red color shows a denser area by electrons, the green shaded area shows the neutral regions on the molecule surface and the blue color area shows less negative potential and more positive potential[57].

RED < YELLOW < GREEN < CYAN < BLUE

It is complementary illustrated from the Figs that all the novel chromophores have better separation of electrophilic and nucleophilic regions highlighting prominent charge separation and transference between donor and acceptor moieties of the chromophores. From all the chromophores, PM3 has greater tendency of negative potential at the substituted acceptor due to presence of highly electron withdrawing ($-NO_2$) acceptor which mainly draws charge tendency towards itself by turning facile charge transfer[58]. In the given visual display of the all molecules the different color regions are vary in every molecule, in the PM3 molecule the red region is greater as compared to all it means that it has higher electrons density, it has good electron with drawing groups are attached which make it more efficient as compared to others. In the PM2 molecule the have less electronegative potential, that's why it has greater blue region in the center of the molecule.

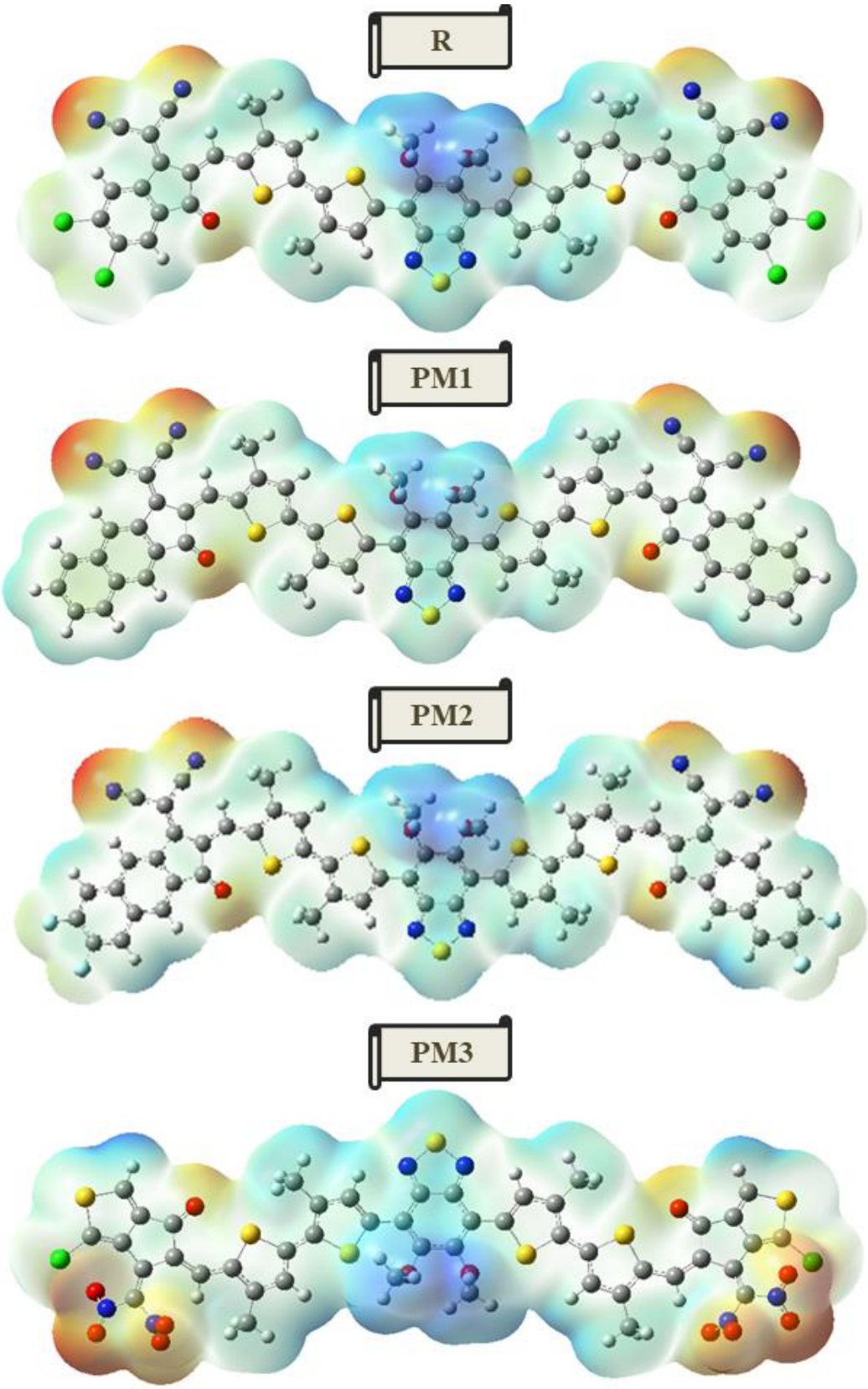
R
PM1
PM2
PM3

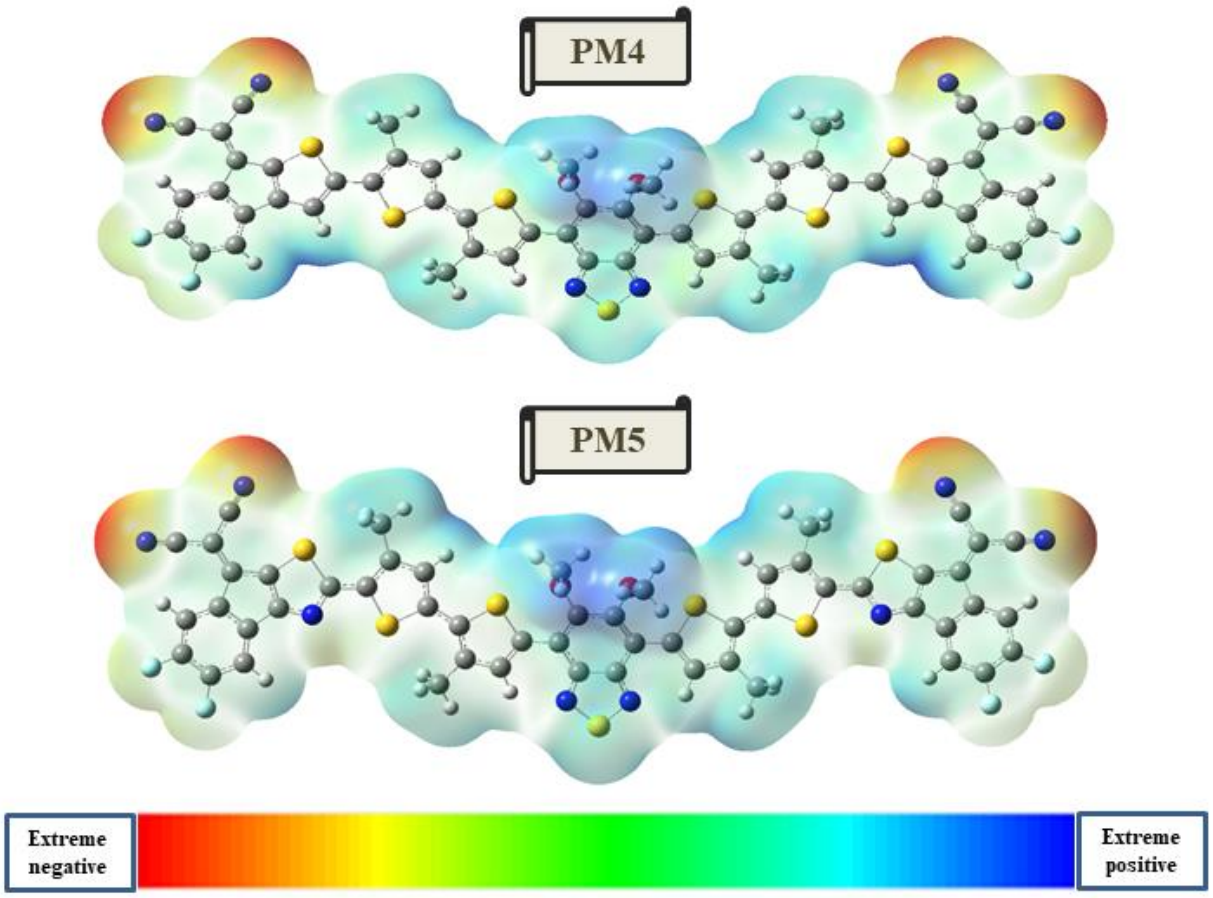

Fig. 7: MEP maps of R and PM1-PM5 highlighting various electrophilic and nucleophilic sites in the chromophores.

Transition Density Matrix (TDM)

The transition density matrix explains the nature of the transition from S_0-S_1 by using the selected functional method of MPW1PW91/6-31G (d,p). The delocalization of the electron-hole pair is analyzed in the S_1 state. TDM explains the localized electrons, holes, and excitations in the molecules from ground to excited states, which help to understand the excitation level of the donors and acceptors. Furthermore, it precisely explains the electron-hole pairs overlapping, charge excitation, the intensity of transition, and diffusion[59]. TDM diagrams witnessed that electrons transfer from the donors towards acceptor units as crucially examined in Fig 8.

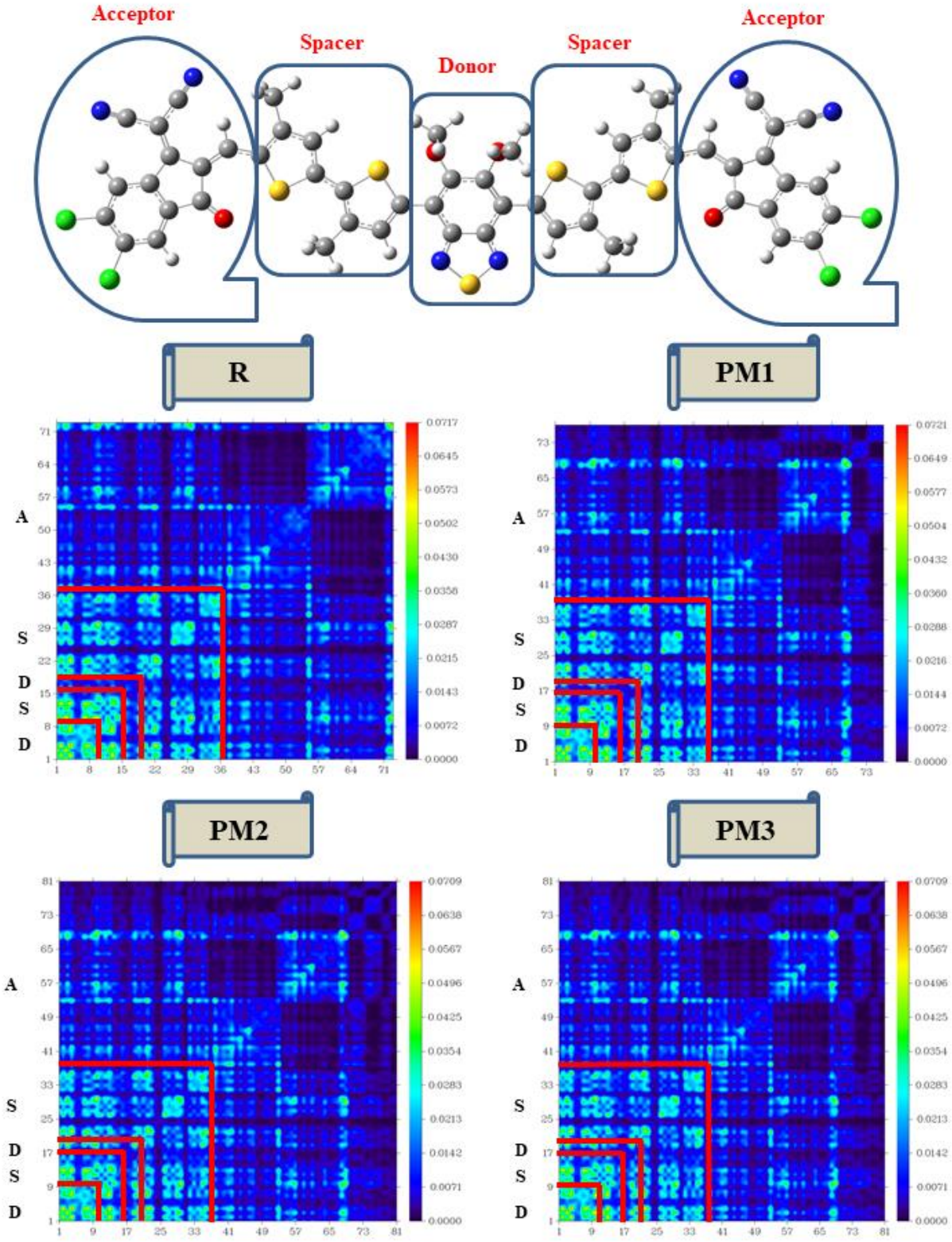
Acceptor
Spacer
Donor
Spacer
Acceptor
R
PM1
PM2
PM3
A
S
D
S
D

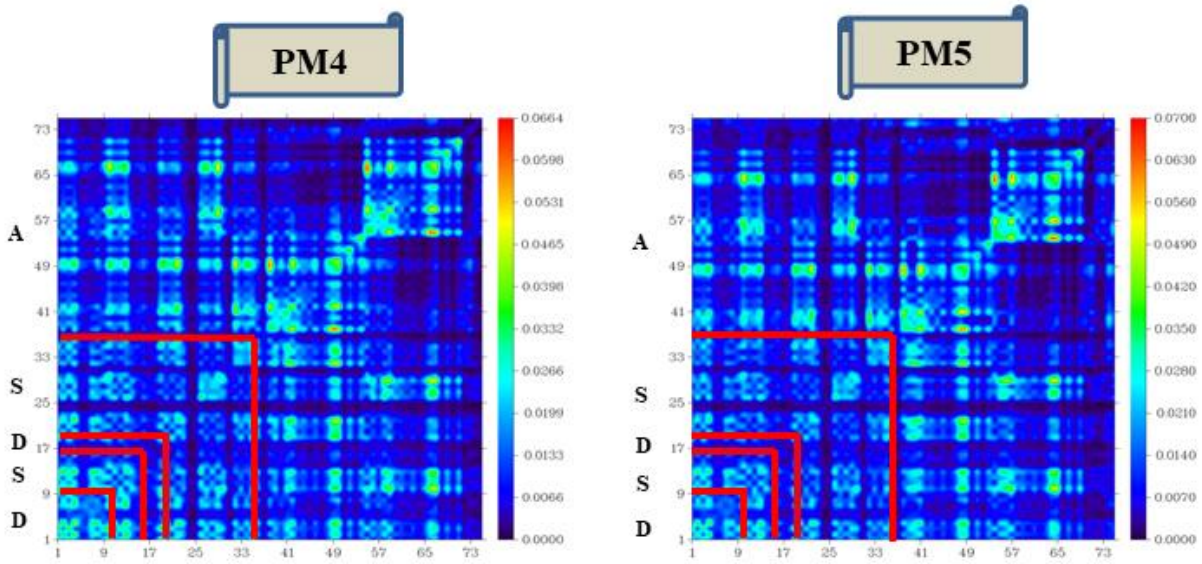

Fig. 8: TDM maps of R and PM1-PM5 for evaluating excitation phenomenon.

In TDM investigation, the contribution of the hydrogen is very small so it is neglected as compared to other connecting atoms having great contribution. In the TDM maps, green and red colors elucidates higher excitation phenomenon, blue hue demonstrates neutral sites while black hue predominantly represents localization phenomenon[60]. From the performed investigation, all the customized chromophores (PM1-PM5) have better excitation potential compared to reference molecule. The red and green hues are present in sufficient quantity predicting their prominent excitation essential for commercialization of solar appliances. Among all planned chromophores, PM3 bestows better excitation phenomenon resulting from stronger electron withdrawing acceptor in the terminal vicinity[61]. In the above given TDM graphs of conceptualized molecules PM3 has the greater hue of the red color which means that PM3 molecule has higher excitation phenomenon as compared to all others molecules which indicates its efficiency. It shows that PM3 has greater efficiency in all the molecules.

Density of State (DOS)

Density of state (DOS) analysis is very crucial factor in solar cell studies as it gives the refining approach to the electronic analysis which creates, refines, and assesses the solar cells. It helps to understand electronic structures, carrier mobility, interference features, and trap states. DOS provides the ranges in which the transitions take place; it explains the total charge states available in the molecules[62]. In the Fig 9, the graphical explanations of the electronic charge density of the acceptors, donors, and core portions are colored different colors. In the graphs, electron volts are taken on the x-axis while relative density is taken on the y-axis. DOS graphs show the percentage contribution of all the parts of the molecule including the acceptors, donors, and core portions[63].

For DOS spectral analysis, PyMolyze 1.1 software is used for the electronic calculations. Researchers are more devoted to comprehending the recombination and trap states to give more comprehension mechanisms due to the DOS analysis. Molecules have intense values of their energy levels (HOMO, LUMO) in the DOS. In the DOS graphs, peaks indicate the electron density of every participant (acceptor, donor, and core) if the electron density of any participant is higher, it will show a strong peak in the DOS graph, if a strong electronegative group is attached then its peak will be at higher level[64]. DOS graphs of the reference molecule (R) as well as the designed molecules (PM1-PM5) are given in Fig 8 which shows different peaks indicating the presence of different electronegative groups of attached acceptors in the molecules. These acceptors having electron-withdrawing groups show the high electron density drawn from the donors' portions of the molecules[65].

The summarized data prescribed in Table 7 demonstrates that HOMO energy level is majorly uplifted through donor moiety while LUMO energy level is affected by substituted acceptors. In all the chromophores, central donor is majorly contributed in contributing to raise HOMO ranging from 60.2 -61.5

%, peripheral acceptors are involving to raise contribution of LUMO in PM1 and PM2 chromophores and their values ranges from 46.8-47.9 % while linking groups (spacers) in involved in uplifting LUMO energy levels in PM3-PM5 molecules ranging from 51.5-80.3 %. To sum up this discussion, it is inferred that HOMO resides mainly on donor vicinity while LUMO resides on linking groups and somewhat on acceptor vicinity[66]. In the given DOS graphs of the all molecules it is concluded that the percentage of the acceptor in the PM2 molecule has high percentage of the contribution which means that the PM2 molecule has attached a good and efficient acceptor which is enhancing its percentage contribution.

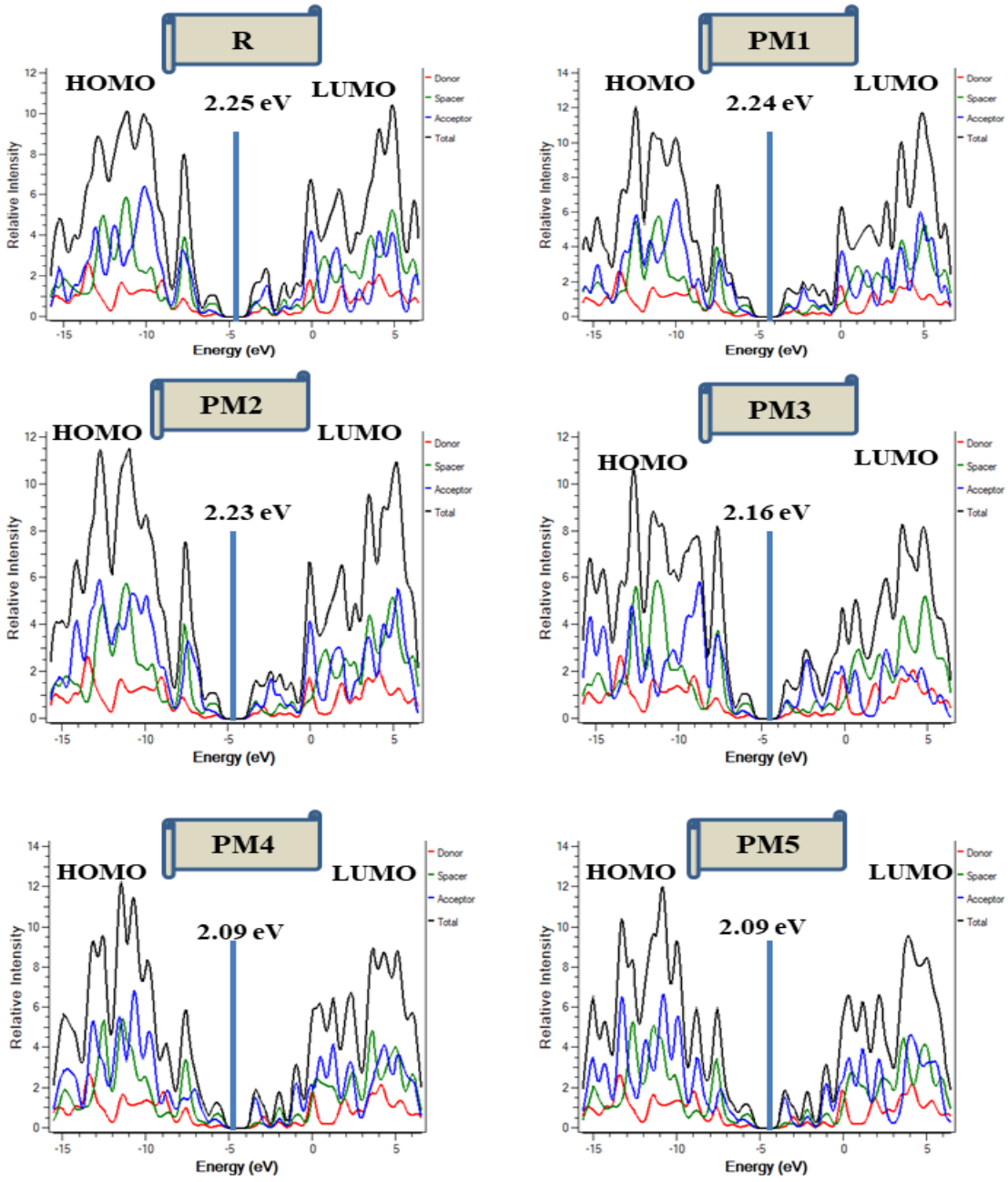

Table-7: Involvement of various molecular fragments (donor, spacer and acceptor) in raising HOMO and LUMO energy levels.

Molecules	Excitation Energy State	Percentage contribution of Donor	Percentage contribution of Spacer	Percentage contribution of Acceptor
R	HOMO	60.8	21.3	17.9
	LUMO	47.9	31.4	20.7
PM1	HOMO	60.4	22.7	16.8
	LUMO	46.8	30.4	22.8
PM2	HOMO	60.2	22.7	17.1
	LUMO	47.3	31.8	20.9
PM3	HOMO	60.7	21.6	17.7
	LUMO	34.4	51.5	14.1
PM4	HOMO	61.2	23.5	15.3
	LUMO	14.9	78.6	6.5
PM5	HOMO	61.5	21.7	16.8
	LUMO	14.6	80.3	5.1

Exciton Binding energy

The evaluation of exciton binding energy is considered as rationale descriptor determining the dissociation of excitons into free charge carriers and their movements towards respective electrodes to assimilate in order to generate electric current. The lower the binding energy of the chromophores, easier will be the segregation of bounded excitons (holes and electrons)[67]. The strongly electronegative acceptors at terminal vicinity resulted in lower Columbic interactions between excitons and results in significant attraction of electrons towards themselves. Following equation 5 is used to estimate statistical values of binding energy[68].

$$E_b = E_g - E_x \quad (5)$$

Here E_g is optical band gap while E_x denotes first excitation energy computed at first excited state. The summarized values of exciton binding energy in gaseous and solvent medium are tabulated in Table 8. The comparable and decreased values of exciton binding energy predict that segregation of excitons in spite of coupling is taking place efficiently resulting in facile transference of charges[69].

Non-covalent Interactions (NCI) and Iso-surfaces

To understand the non-covalent interaction (NCI) and iso-surfaces, structures and graphs are plotted using Multiwfn 3.8 software by the reduced density gradient factor. NCI graphs help to understand the repulsive interaction or steric hindrance and the attractive interactions as wander walls forces, hydrogen bonding, and other interactions due to electronegative atoms (S, O)[70]. For the NCI graphs, we have taken the product of energy and second value (sign(λ)ρ) on the x-axis and the reduced density gradient (RDG) is taken on the y-axis. NCI graphs explained the different interactions present in the molecules in the form of different colors such as blue, green, and red color[71]. The green color shows the presence of van der Waals interactions within the molecules which shows weak interactions, blue color shows the presence of hydrogen bonding and attractive forces within the molecules, while the red color shows the repulsive interactions in the molecule as highlighted in Fig 10[72].

Table-8: Statistical calculations of exciton binding energy for R and PM1-PM5 in solvent and gaseous phases.

Molecules	E_g (eV)	E_b (solvent)	E_b (gaseous)
R	**2.25**	**0.49**	**0.40**
PM1	**2.24**	**0.48**	**0.41**
PM2	**2.23**	**0.48**	**0.40**
PM3	**2.16**	**0.50**	**0.38**
PM4	**2.09**	**0.49**	**0.37**
PM5	**2.09**	**0.49**	**0.37**

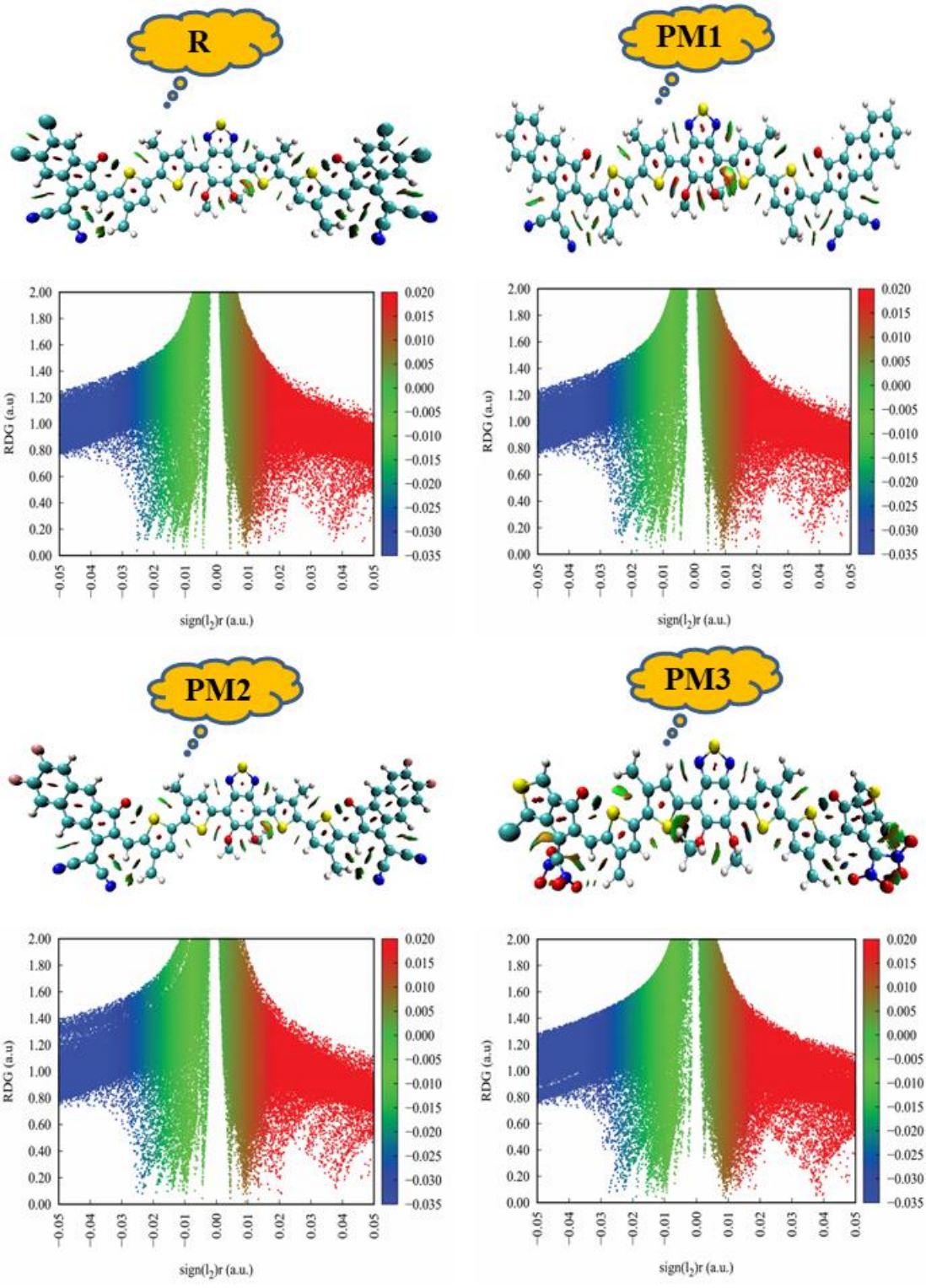
R
PM1
PM2
PM3
RDG (a.u)
sign(l2)r (a.u.)

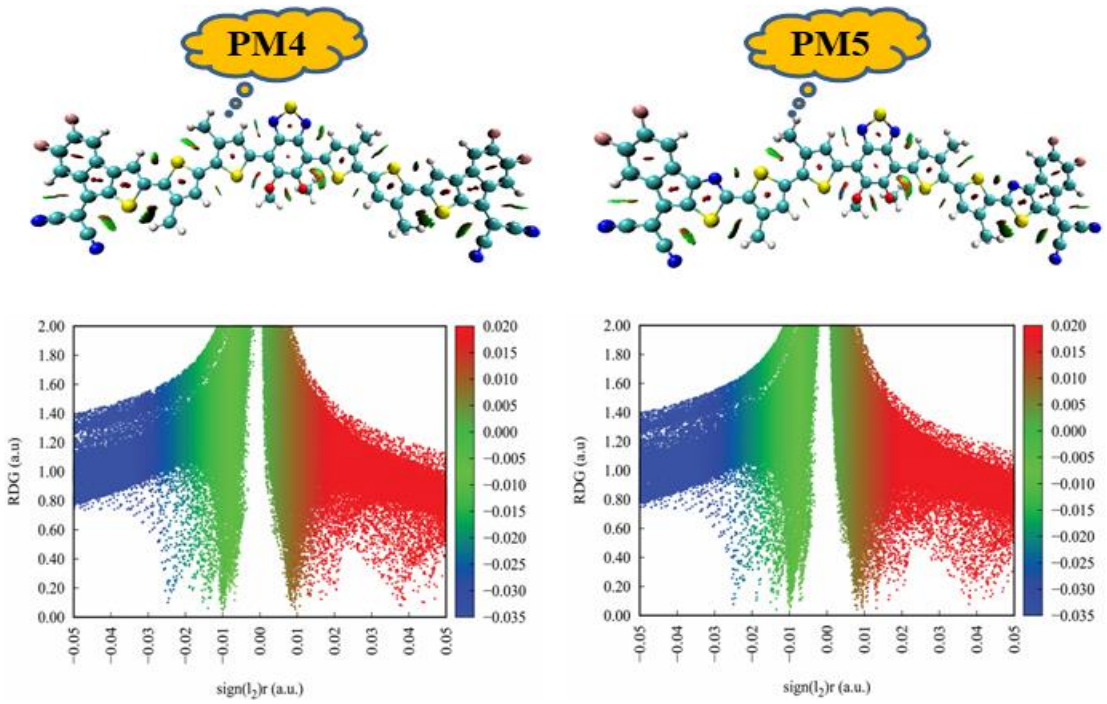

Fig 10: NCI maps and iso-surfaces plotted through RDG software and Multiwfn software

On the y-axis, the graph has a negative value because hydrogen bonding is present due to the presence of electronegative atoms as the electronegativity increases within the molecule the peak spreads towards the negative value, which is witnessed that hydrogen bonding is present[73]. The presence of strong non-covalent interactions in the graphs of newly designed molecules indicates having electronegative atoms in the molecules, the presence of H-bonding is shown by the blue in the NCI graphs. The green in the middle of the graphs shows the van der Waals forces are present in the molecules, as the van der Waals forces increase, green color spreads more over the graph[74].

From the NCI maps, it is clear that blue line is present above than the red line suggesting that attractive forces are dominating compared to repulsive forces. The presence of blue color spikes at higher position demonstrates the stable character of chromophores which is essential criterion for proficiency[75].

Dipole Moment

In order to understand crystalline behavior, orderliness, solubility and accommodation of charges, evaluation of dipole moment is vital. As the light falls on solar cells and they absorb sufficient quantity of light, the phenomenon of the separation of positive and negative charges takes place; the separation of these charges makes an electric field and creates diploes within the molecules[76]. The dipole moment (DP) denoted as μ helps to understand how much chromophores are soluble in the organic solvent. The solubility has direct association with the dipole moment; hence, solubility increases as the dipole moment increases. Greater dipole moment will help to increase the solvent processibility and better crystal formation[77].

The evaluation of dipole moment is performed in both gaseous and solvent mediums at best elected MPW1PW91 functional with 6-31 G (d,p) methodology[78]. The decreasing order of dipole moment in both mediums is; PM1 > PM4 > PM3 > PM2 > R > PM5. On the basis of conFigd calculations, all customized molecules has the highest dipole moment as compared to reference molecule, highlighting their greater ability of dissolution in the solvent medium which helps to increase the solvent processibility which make better crystals[79].

Reorganization energy

Reorganization energy (RE) has a significant role in the charge transfer, transport, and performance of solar devices. RE is associated with non-radiative recombination, the major factor affecting the energy losses in organic photovoltaic cells. In this project, reorganization energy is the main parameter used to calculate the efficiency of the organic solar cells[80]. RE is divided into internal reorganization energy (IR)

and external reorganization energy (ER). The IR deals with the electronic states in the ground and excited states and the ER is concerned with external factors such as solvation, temperature, polarization, and other external factors. As there is no change occurring in the external environment there is no change in ER therefore, it is neglected. In this project, we mainly focused on the IR because the hole (λ_{h+} λ_{+}) and electron (λ_e + λ) reorganization energies make up the internal energies due to charge transfer[81].

The internal reorganization energy is the combination of the hole (λ_{h+} λ_{+}) and electrons. The charge mobility has an inverse relation with reorganization energy, lower the reorganization energy, facile will be charge movement and vice-versa. The computed values summarized in Table 9 suggest that computed molecules have better hole transporting ability owing to lower reorganization energy of holes and electrons which suggest that all customized molecules performed well in solar appliances[82].

Table-9: Concised values of reorganization energy of electron and holes for the reference and investigated compounds (PM1-PM5)

Molecules	λ_e (electron)	λ_h (hole)
R	**0.060186**	**0.066321**
PM1	**0.047291**	**0.047814**
PM2	**0.056129**	**0.061084**
PM3	**0.162140**	**0.106114**
PM4	**0.069841**	**0.062932**
PM5	**0.074296**	**0.069410**

Light Harvesting Efficiency

Light harvesting efficiency (LHE) is another crucial factor in determining OSCs' photocurrent and optical efficiency. It is the capability of solar devices to absorb solar radiation and harvest them to generate valuable photocurrent[83]. When the LHE is high, a huge quantity of circuit current is produced, which also magnifies the molecules' photocurrent response. The following equation 6 is used to calculate the LHE of the molecules in solar cell devices[84].

$$LHE = 1\text{-}10^{-f} \qquad (6)$$

When the transition of electrons from one energy level to another occurs by the emission and absorption of the radiation, the LHE is determined through oscillator strength (f_{OS}). LHE of the reference molecule (R) and designed molecules (PM1-PM5) in gaseous and solvent phase are predominantly given in Table 10. LHE is directly correlated with oscillator strength indicating that elevated oscillator strength up-scales harvesting of radiations from the sun to generate electricity and vice-versa[85].

Table-10: Summarized values of light harvesting efficiency of all customized chromophores in both solvent and gaseous mediums

Molecules	LHE (Solvent)	LHE (Gaseous)
R	**0.999206**	**0.998287**
PM1	**0.999445**	**0.998623**
PM2	**0.999459**	**0.998733**
PM3	**0.998485**	**0.997255**
PM4	**0.993017**	**0.989375**
PM5	**0.988607**	**0.984307**

The reference and the designed molecule are arranged in ascending order PM2 > PM1 > R > PM3 > PM4 > PM5. From the evaluated results PM1 and PM2 has the highest LHE which indicates that these chromophores have an intensified peak of absorption highlighting their proficiency in solar appliances[83].

Open Circuit Voltage (V_{OC})

Open circuit voltage is the total output of solar devices when the applied current is zero. V_{OC} is a crucial factor in the investigation of the power conversion efficiency of solar cells. It is critically influenced through various parameters like energy level of material, light source, temperature, recombination of charge carriers, light intensity and device morphology[86]. For calculation of open circuit voltage, LUMO of acceptor and HOMO of donor molecule is under scored. All the scrutinized chromophores are blended with $PC_{61}BM$ acceptor whose HOMO value is -5.10 eV while LUMO value is -3.90 eV. The theoretical estimation of open circuit voltage is executed from the equation 7 formulated by Scharber and his colleagues[87].

$$V_{OC} = \frac{1}{e}\left[E_{\text{LUMO OF THE ACCEPTOR}} - E_{\text{HOMO OF THE DONOR}}\right] - 0.3 \qquad (7)$$

Here, e is designated the molecular charge while 0.3 is the constant parameter calculated from the drop voltage resulting from the mechanisms of radiative loss, recombination loss and during energy transfer. For attaining increased V_{OC}, donor's HOMO must be at lower energy level while acceptor's LUMO has higher energy level[88]. The computed V_{OC} of the reference molecule is 1.59 eV while all the scrutinized molecules have open circuit voltage ranging from 1.56-1.34 eV prescribed in Table 10. The declining trend of V_{OC} is; R > PM3 > PM2 > PM5 > PM1 > PM4[88]. It is visualized from Fig 11 that all the planned molecules have comparable values of V_{OC} with model molecule indicating their comparable efficiency suggesting that they should be developed synthetically for potential applications in generation of current[89].

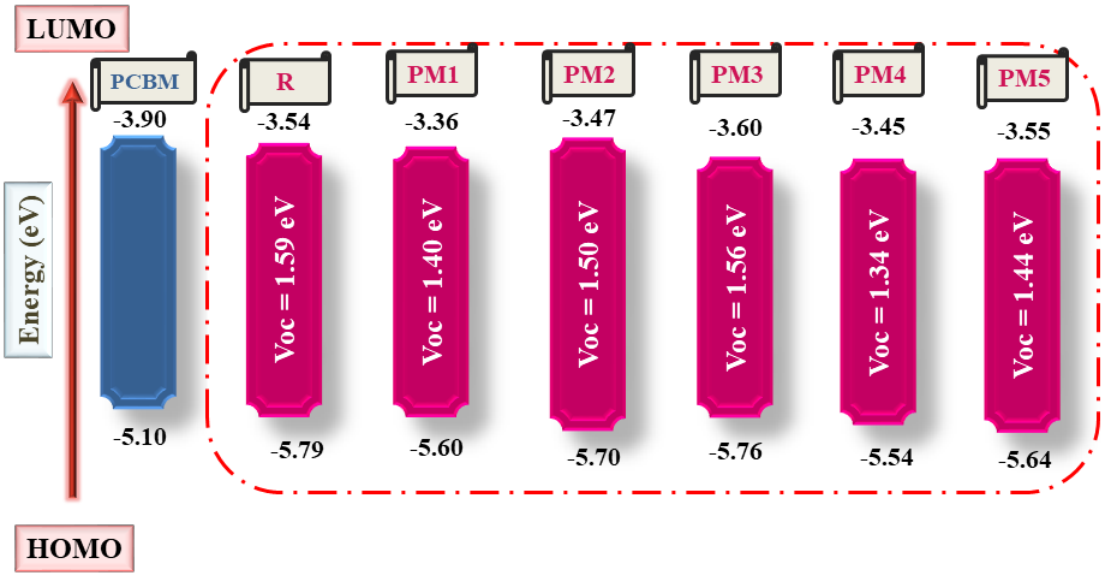

Fig. 11: Portray of V_{OC} visualization computed by blending all investigated chromophores with PCBM acceptor.

Table-11: Calculated values of various photovoltaic parameters (V_{OC}, Normalized V_{OC}, FF) for R and customized molecules (PM1-PM5).

Molecules	V_{OC} (eV)	Normalized V_{OC}	Fill Factor (FF)
R	1.59	61.5063	0.917916
PM1	1.40	54.1565	0.909256
PM2	1.50	58.0248	0.914049
PM3	1.56	60.3458	0.916669
PM4	1.34	51.8355	0.906088
PM5	1.44	55.7038	0.911242

Fill Factor Analysis (FF)

Fill factor (FF) is another vital tool to explain the conversion of light to electricity to explain the efficiency of photovoltaic devices. It is the dimensionless quantity which depends on the open circuit voltage, higher the V_{OC} higher the FF and vice versa[90]. The conversion of the incoming light into electrical energy determining effectiveness of the device is calculated by the fill factor. Furthermore, fill factor has direct effects on the power conversion efficiency of the solar cell by minimizing energy losses due to quality determining of the exciton extractions. The theoretical calculation of fill factor is performed utilizing equation 8[91].

$$FF = \frac{e^{\frac{Voc}{K_B T}} - \ln\left(e^{\frac{Voc}{K_B T}} + 0.72\right)}{e^{\frac{Voc}{K_B T}} + 1} \qquad (8)$$

Here e represents elementary charge, T denotes absolute temperature (300 K), K_B highlights Boltzmann constant and $e^{\frac{Voc}{K_B T}}$ is mentioned as normalized V_{OC}. The statistical values of fill factor are concised in Table 11 which suggest that all chromophores have comparable values of fill factor which are required for stable and most efficient solar devices[92].

Power Conversion Efficiency (PCE)

PCE defines the overall efficiency of the OSCs and it is the ratio between the output energy and input energy which measures the conversion of power from solar radiations to electricity[5]. In the OSCs, main feature on which the activity of OSCs depends is the power conversion efficiency (PCE) which mainly concerns with the fill factor, short circuit current density, and open circuit voltage. PCE is essentially calculated using the equation 9[93].

$$PCE = J_{SC}\, V_{OC}\, FF / P_{in} \qquad (9)$$

In this equation J_{SC} represents short circuit voltage, FF is fill factor, V_{OC} is open circuit voltage, and P_{in} is the incident light. The comparable values of open circuit voltage and fill factor suggest that all chromophores have enhanced power conversion

efficiency and suggested as efficient solar cells to be synthesized developed in new era of solar technologies[94].

Conclusion

The development of organic solar cells with low band gap and robust open circuit voltage is cutting edge task for all research community. To obtain promising outcomes, various methodologies are being utilized through various amendments in molecular geometry. In recent research approach, reference molecule is amended through end-capped modification and various parameters are elucidated by selecting appropriate MPW1PW91 functional in careful manner. Through computational analysis, reduced band gap ranging from 2.09-2.24 eV, bathochromic shift in absorption (706-776 nm in chloroform solvent and 676-721 nm in gaseous media), lowest excitation energy (1.60-1.76 eV) was obtained. Furthermore, devised chromophores upsurge excellent dipole moment upto 13.22 D predicting their better solubility and crystallinity in solvent medium. The customized molecules have lower reorganization energy of holes and electrons and comparable open circuit voltage recommend them best adaptable hole transporting materials in solar gadgets with sufficiently enhanced power conversion efficiency.

Acknowledgment

The experiments presented in this paper were partially carried out using the facilities of the Benefit Advanced AI and Computing Lab at the University of Bahrain (https://ailab.uob.edu.bh) with support from Benefit Bahrain Company (https://benefit.bh).

References

1. Jeon, S.J., et al., *Molecular design of cost-effective donor polymers with high visible transmission for eco-friendly and efficient semitransparent organic solar cells.* Chemical Engineering Journal, 2023. **472**: p. 144850.
2. Awogbemi, O. and D.V. Von Kallon, *Towards the development of underutilized renewable energy resources in achieving carbon neutrality.* Fuel Communications, 2023: p. 100099.
3. Luo, B., D. Ye, and L. Wang, *Recent progress on integrated energy conversion and storage systems.* Advanced Science, 2017. **4**(9): p. 1700104.
4. Zhou, H., T. Fan, and D. Zhang, *Biotemplated materials for sustainable energy and environment: current status and challenges.* ChemSusChem, 2011. **4**(10): p. 1344-1387.
5. Yun, S., et al., *New-generation integrated devices based on dye-sensitized and perovskite solar cells.* Energy & Environmental Science, 2018. **11**(3): p. 476-526.
6. Scharber, M.C. and N.S. Sariciftci, *Efficiency of bulk-heterojunction organic solar cells.* Progress in polymer science, 2013. **38**(12): p. 1929-1940.
7. Park, C.-G., J.d.C. Pérez, and B. Ratra, *Using non-DESI data to confirm and strengthen the DESI 2024 spatially flat w 0 wa CDM cosmological parametrization result.* Physical Review D, 2024. **110**(12): p. 123533.
8. Moon, J.S., et al., *2023 clinical practice guidelines for diabetes management in Korea: full version recommendation of the Korean diabetes association.* Diabetes & Metabolism Journal, 2024. **48**(4): p. 546-708.
9. Yan, C., et al., *Non-fullerene acceptors for organic solar cells.* Nature Reviews Materials, 2018. **3**(3): p. 1-19.
10. Zhang, Y., *Investigation of high-performance non-fullerene organic solar cells prepared with novel nanostructures.* 2022.
11. Ng, C., et al., *Photovoltaic performances of mono- and mixed-halide structures for perovskite solar cell: A review.* Renewable and Sustainable Energy Reviews, 2018. **90**: p. 248-274.
12. Wadsworth, A., et al., *Critical review of the molecular design progress in non-fullerene electron acceptors towards commercially viable organic solar cells.* Chemical Society Reviews, 2019. **48**(6): p. 1596-1625.
13. 13. Wang, J., et al., *The principles, design and applications of fused-ring electron acceptors.* Nature Reviews Chemistry, 2022. **6**(9): p. 614-634.
14. Prins, L.J., D.N. Reinhoudt, and P. Timmerman, *Noncovalent synthesis using hydrogen bonding.* Angewandte Chemie International Edition, 2001. **40**(13): p. 2382-2426.
15. Huang, H., et al., *Organic and polymeric semiconductors enhanced by noncovalent conformational locks.* Chemical reviews, 2017. **117**(15): p. 10291-10318.
16. Luo, D., C.J. Brabec, and A.K.K. Kyaw, *Non-fused ring electron acceptors for high-performance and low-cost organic solar cells: Structure-function, stability and synthesis complexity analysis.* Nano Energy, 2023: p. 108661.
17. Jiang, P., et al., *Emergence of Low-Cost and High-Performance Nonfused Ring Electron Acceptors.* Accounts of Chemical Research, 2024. **57**(23): p. 3419-3432.
18. Bai, Q., et al., *Recent progress in low-cost noncovalently fused-ring electron acceptors for organic solar cells: Special Issue: Emerging Investigators.* Aggregate, 2022. **3**(6): p. e281.
19. Peng, H.-Q., et al., *Biological applications of supramolecular assemblies designed for excitation*

energy transfer. Chemical reviews, 2015. **115**(15): p. 7502-7542.
20. Yao, H., et al., *Molecular design of benzodithiophene-based organic photovoltaic materials.* Chemical reviews, 2016. **116**(12): p. 7397-7457.
21. Ye, L., et al., *Molecular design toward highly efficient photovoltaic polymers based on two-dimensional conjugated benzodithiophene.* Accounts of chemical research, 2014. **47**(5): p. 1595-1603.
22. Li, Y., *Molecular design of photovoltaic materials for polymer solar cells: toward suitable electronic energy levels and broad absorption.* Accounts of chemical research, 2012. **45**(5): p. 723-733.
23. Li, Q. and Z. Li, *Molecular packing: another key point for the performance of organic and polymeric optoelectronic materials.* Accounts of chemical research, 2020. **53**(4): p. 962-973.
24. Han, C., et al., *Two Completely Non-Fused Ring Acceptors Working in an Alloy-Like Model for Efficient and Stable Organic Solar Cells.* Advanced Energy Materials, 2024. **14**(17): p. 2304063.
25. Ma, Q., et al., *One-step dual-additive passivated wide-bandgap perovskites to realize 44.72%-efficient indoor photovoltaics.* Energy & Environmental Science, 2024. **17**(5): p. 1637-1644.
26. Li, H., et al., *Ethanol Processable Inorganic-Organic Hybrid Hole Transporting Layers Enabled 20.12% Efficiency Organic Solar Cells.* Angewandte Chemie International Edition, 2025. **64**(4): p. e202416866.
27. Hassan, E.M., Y.F. Mustafa, and M.M. Merkhan, *Computation in chemistry: representative software and resources.* Int J Pharmacy Pharm St, 2022. **6**(2): p. 1-10.
28. Kumar, V., J. Teotia, and A.K. Yadav, *Vibrational (FT-Raman and FTIR) spectroscopic study, molecular structure, thermodynamic properties and non-linear optical properties of benzyl-3-oxopyperazine-1-carboxylate by density functional theory.* Materials Today: Proceedings, 2022. **62**: p. 7137-7141.
29. Caricato, M., et al., *Gaussian 09: IOps Reference*. 2009: Gaussian Wallingford, CT, USA.
30. Laurent, A.D. and D. Jacquemin, *TD-DFT benchmarks: a review.* International Journal of Quantum Chemistry, 2013. **113**(17): p. 2019-2039.
31. Ubaldo, P. and L. Wang, *Comparative DFT Studies of Optoelectronic Properties of MTPA Derivatives.* 2024.
32. Mohan, N., et al., *Comparison of aromatic NH··· π, OH··· π, and CH··· π interactions of alanine using MP2, CCSD, and DFT methods.* Journal of computational chemistry, 2010. **31**(16): p. 2874-2882.
33. Waisman, E. and J.L. Lebowitz, *Mean spherical model integral equation for charged hard spheres I. Method of solution.* The Journal of Chemical Physics, 1972. **56**(6): p. 3086-3093.
34. Halliwell, J.J. and R.C. Myers, *Multiple-sphere configurations in the path-integral representation of the wave function of the universe.* Physical Review D, 1989. **40**(12): p. 4011.
35. Baker, J.A., *Integration over spheres and the divergence theorem for balls.* The American mathematical monthly, 1997. **104**(1): p. 36-47.
36. Waisman, E. and J.L. Lebowitz, *Mean spherical model integral equation for charged hard spheres. II. Results.* The Journal of Chemical Physics, 1972. **56**(6): p. 3093-3099.
37. Zhang, J., et al., *Material insights and challenges for non-fullerene organic solar cells based on small molecular acceptors.* Nature Energy, 2018. **3**(9): p. 720-731.
38. Zhang, G., et al., *Nonfullerene acceptor molecules for bulk heterojunction organic solar cells.* Chemical reviews, 2018. **118**(7): p. 3447-3507.
39. Luo, D., C.J. Brabec, and A.K.K. Kyaw, *Non-fused ring electron acceptors for high-performance and low-cost organic solar cells: Structure-function, stability and synthesis complexity analysis.* Nano Energy, 2023. **114**: p. 108661.
40. Wodo, O. and B. Ganapathysubramanian, *Modeling morphology evolution during solvent-based fabrication of organic solar cells.* Computational Materials Science, 2012. **55**: p. 113-126.
41. Sengupta, A., et al., *Cycloaddition reactivities analyzed by energy decomposition analyses and the frontier molecular orbital model.* Accounts of Chemical Research, 2022. **55**(17): p. 2467-2479.
42. Yu, J., N.Q. Su, and W. Yang, *Describing chemical reactivity with frontier molecular orbitalets.* JACS au, 2022. **2**(6): p. 1383-1394.
43. Braga, L.S., et al., *Perspectives on the role of the frontier effective-for-reaction molecular orbital (FERMO) in the study of chemical reactivity: an updated review.* Current Organic Chemistry, 2020. **24**(3): p. 314-331.
44. Vinduja, P., et al., *A Computational Modeling of the Structure, Frontier Molecular Orbital (FMO) Analysis, and Global and Local Reactive Descriptors of a Phytochemical 'Coumestrol'*, in *Mathematics Applied to Engineering in Action*. 2021, Apple Academic Press. p. 41-60.
45. Markovic, S. and J. Tosovic, *Application of time-dependent density functional and natural bond orbital theories to the UV–vis absorption spectra of some phenolic compounds.* The Journal of Physical Chemistry A, 2015. **119**(35): p. 9352-9362.
46. Li, J.-H., et al., *Identifying and tracing potential energy surfaces of electronic excitations with*

specific character via their transition origins: application to oxirane. Physical Chemistry Chemical Physics, 2015. **17**(18): p. 12065-12079.
47. Zheng, L., et al., *Where is the electronic oscillator strength? Mapping oscillator strength across molecular absorption spectra*. The Journal of Physical Chemistry A, 2016. **120**(11): p. 1933-1943.
48. Hannaford, P., *The oscillator strength in atomic absorption spectroscopy.* Spectrochimica Acta Part B: Atomic Spectroscopy, 1994. **49**(12-14): p. 1581-1593.
49. Masselink, W., et al., *Absorption coefficients and exciton oscillator strengths in AlGaAs-GaAs superlattices.* Physical Review B, 1985. **32**(12): p. 8027.
50. van der Poel, W., L. Molenkamp, and C. Foxon, *Giant oscillator strength of free excitons in GaAs.* Physical Review B, 1987. **35**(15): p. 8281.
51. Thomas, R., et al., *Plexcitons: the role of oscillator strengths and spectral widths in determining strong coupling.* ACS nano, 2018. **12**(1): p. 402-415.
52. Woolley, R., *Oscillator strengths and the continuous absorption coefficient.* Monthly Notices of the Royal Astronomical Society, Vol. 95, p. 101, 1934. **95**: p. 101.
53. Chan, W., et al., *Absolute optical oscillator strengths for the electronic excitation of atoms at high resolution. II. The photoabsorption of neon.* Physical Review A, 1992. **45**(3): p. 1420.
54. Wemple, S., *Optical oscillator strengths and excitation energies in solids, liquids, and molecules.* The Journal of Chemical Physics, 1977. **67**(5): p. 2151-2168.
55. You, Z.Q. and C.P. Hsu, *Theory and calculation for the electronic coupling in excitation energy transfer.* International Journal of Quantum Chemistry, 2014. **114**(2): p. 102-115.
56. Lakshminarayanan, S., et al., *Molecular electrostatic potential (MEP) surface analysis of chemo sensors: An extra supporting hand for strength, selectivity & non-traditional interactions.* Journal of Photochemistry and Photobiology, 2021. **6**: p. 100022.
57. Pullman, A. and B. Pullman, *Molecular electrostatic potential of the nucleic acids.* Quarterly reviews of biophysics, 1981. **14**(3): p. 289-380.
58. Luque, F., et al., *SCRF calculation of the effect of water on the topology of the molecular electrostatic potential.* The Journal of Physical Chemistry, 1993. **97**(37): p. 9380-9384.
59. Wang, L., et al., *The role of the natural transition orbital density in the S0→ S1 and S0→ S2 transitions of fulvene with next generation QTAIM.* Chemical Physics Letters, 2020. **751**: p. 137556.
60. Vishwanath, A., L. Balents, and T. Senthil, *Quantum criticality and deconfinement in phase transitions between valence bond solids.* Physical Review B—Condensed Matter and Materials Physics, 2004. **69**(22): p. 224416.
61. Kühn, O. and V. Sundström, *Pump–probe spectroscopy of dissipative energy transfer dynamics in photosynthetic antenna complexes: A density matrix approach.* The Journal of chemical physics, 1997. **107**(11): p. 4154-4164.
62. Wang, Y., et al., *Density functional theory analysis of structural and electronic properties of orthorhombic perovskite CH 3 NH 3 PbI 3*. Physical Chemistry Chemical Physics, 2014. **16**(4): p. 1424-1429.
63. Nadenau, V., et al., *Electronic properties of CuGaSe 2-based heterojunction solar cells. Part I. Transport analysis.* Journal of Applied Physics, 2000. **87**(1): p. 584-593.
64. Shafiq, F., et al., *Star-shaped small donor molecules based on benzotriindole for efficient organic solar cells: A DFT study.* Journal of Molecular Modeling, 2024. **30**(3): p. 76.
65. Rahman, B.S.M., *Study of Structure, Band, and Density of States Properties of $TlPbCl_3$ with DFT Based on First-Principles Calculations*. Department of Physics, Bangabandhu Sheikh Mujibur Rahman Science and ….
66. Von Hauff, E. and D. Klotz, *Impedance spectroscopy for perovskite solar cells: characterisation, analysis, and diagnosis.* Journal of Materials Chemistry C, 2022. **10**(2): p. 742-761.
67. Zhu, L., Y. Yi, and Z. Wei, *Exciton binding energies of nonfullerene small molecule acceptors: implication for exciton dissociation driving forces in organic solar cells.* The Journal of Physical Chemistry C, 2018. **122**(39): p. 22309-22316.
68. Kraner, S., G. Prampolini, and G. Cuniberti, *Exciton binding energy in molecular triads.* The Journal of Physical Chemistry C, 2017. **121**(32): p. 17088-17095.
69. Bombile, J.H., M.J. Janik, and S.T. Milner, *Energetics of exciton binding and dissociation in polythiophenes: A tight binding approach*. Physical Chemistry Chemical Physics, 2019. **21**(22): p. 11999-12011.
70. Medimagh, M., et al., *Impact of non-covalent interactions on FT-IR spectrum and properties of 4-methylbenzylammonium nitrate. A DFT and molecular docking study*. Heliyon, 2021. **7**(10).
71. Tsering, D., et al., *Combined experimental and theoretical studies of Quinoxalinone-based Spiropyrrolidines: Estimation of non-covalent interactions.* Journal of Molecular Structure, 2024. **1318**: p. 139343.
72. Ullah, Z., et al., *Computational study of Pd–Cd bimetallic crystals: spectroscopic properties, hirshfeld surface analysis, non-covalent interaction,*

and sensor activity. Journal of Molecular Liquids, 2022. **365**: p. 120111.
73. Rizwan, H.A., et al., *Deciphering the adsorption and sensing performance of Al24N24 and B24N24 nanoclusters as a drug delivery system for nitrosourea anticancer drug: A DFT insight.* Surfaces and Interfaces, 2024. **51**: p. 104779.
74. Dappe, Y.J. and J.I. Martínez, *Effect of van der Waals forces on the stacking of coronenes encapsulated in a single-wall carbon nanotube and many-body excitation spectrum.* Carbon, 2013. **54**: p. 113-123.
75. Black, W., et al., *Measurements of retarded Van Der Waals' forces.* Transactions of the Faraday Society, 1960. **56**: p. 1597-1608.
76. Terenziani, F., et al., *Enhanced two-photon absorption of organic chromophores: theoretical and experimental assessments.* Advanced Materials, 2008. **20**(24): p. 4641-4678.
77. Khan, M.U., et al., *Predicting benzodithiophene based donor materials with enhanced 19.09% PCE, open-circuit voltage and optoelectronic attributes for solar cell applications: Photochemical insights from DFT*. Journal of Photochemistry and Photobiology A: Chemistry, 2024. **446**: p. 115115.
78. Khan, M.I., et al., *Quantum mechanical modeling of fused rings-based small-donor molecules with enhanced optoelectronic attributes for high performance organic photovoltaic cells.* Journal of Physics and Chemistry of Solids, 2023. **174**: p. 111140.
79. Jędrzejewska, B., et al., *Styryl dye possessing donor-π-acceptor structure–synthesis, spectroscopic and computational studies.* Dyes and Pigments, 2013. **99**(3): p. 673-685.
80. Oliveira, E.F. and F.C. Lavarda, *Reorganization energy for hole and electron transfer of poly (3-hexylthiophene) derivatives.* Polymer, 2016. **99**: p. 105-111.
81. Matyushov, D.V., *Reorganization energy of electron transfer.* Physical Chemistry Chemical Physics, 2023. **25**(11): p. 7589-7610.
82. Katubi, K.M., et al., *Machine learning assisted designing of organic semiconductors for organic solar cells: High-throughput screening and reorganization energy prediction.* Inorganic Chemistry Communications, 2023. **151**: p. 110610.
83. Ompong, D., M. Narayan, and J. Singh, *Optimization of photocurrent in bulk heterojunction organic solar cells using optical admittance analysis method.* Journal of Materials Science: Materials in Electronics, 2017. **28**: p. 7100-7106.
84. Luo, G., et al., *Recent advances in organic photovoltaics: device structure and optical engineering optimization on the nanoscale.* Small, 2016. **12**(12): p. 1547-1571.
85. Ryu, S., et al., *Light intensity dependence of organic solar cell operation and dominance switching between Shockley–Read–Hall and bimolecular recombination losses.* Scientific reports, 2021. **11**(1): p. 16781.
86. Elumalai, N.K. and A. Uddin, *Open circuit voltage of organic solar cells: an in-depth review.* Energy & Environmental Science, 2016. **9**(2): p. 391-410.
87. Azzouzi, M., T. Kirchartz, and J. Nelson, *Factors controlling open-circuit voltage losses in organic solar cells.* Trends in Chemistry, 2019. **1**(1): p. 49-62.
88. Qi, B. and J. Wang, *Open-circuit voltage in organic solar cells.* Journal of Materials Chemistry, 2012. **22**(46): p. 24315-24325.
89. Xue, Q., et al., *Dual interfacial modifications enable high performance semitransparent perovskite solar cells with large open circuit voltage and fill factor.* Advanced Energy Materials, 2017. **7**(9): p. 1602333.
90. Wang, D., et al., *How to minimize voltage and fill factor losses to achieve over 20% efficiency lead chalcogenide quantum dot solar cells: Strategies expected through numerical simulation.* Applied Energy, 2023. **341**: p. 121124.
91. Chiyesu, S., *Outdoor testing of some commercial solar panels found on the Zambian market in terms of their fill-factor and efficiency*. 2023, The University of Zambia.
92. Khattak, Y.H., *Modeling of high power conversion efficiency thin film solar cells*. 2019, Universitat Politècnica de València.
93. Chong, K.-K., et al., *Comprehensive method for analyzing the power conversion efficiency of organic solar cells under different spectral irradiances considering both photonic and electrical characteristics.* Applied Energy, 2016. **180**: p. 516-523.
94. Marzouglal, M., et al., *Prediction of power conversion efficiency parameter of inverted organic solar cells using artificial intelligence techniques.* Scientific Reports, 2024. **14**(1): p. 25931.